UNIVERSITY OF CALIFORNIA
RIVERSIDE

Removal of Engineered Nanomaterials Through Conventional Water Treatment Processes

A Dissertation submitted in partial satisfaction
of the requirements for the degree of

Doctor of Philosophy

in

Chemical and Environmental Engineering

by

Ryan James Honda

August 2014

Dissertation Committee:
Dr. Sharon L. Walker, Chairperson
Dr. Mark R. Matsumoto
Dr. David Jassby

The Dissertation of Ryan James Honda is approved:

Committee Chairperson

University of California, Riverside

Acknowledgments

I would first like to thank my advisor, Dr. Sharon L. Walker, for her wonderful guidance, support, and motivation throughout my PhD career. My dissertation would not have been possible without her tremendous and selfless amount of time, effort, and dedication in mentoring me from the beginning to the end of my doctoral research. Due to her vast knowledge and creativity in Chemical and Environmental Engineering, I was able to not only gain a deeper understanding in Water Quality Systems Control, but also develop a greater appreciation for the field, which heightened my passion to pursue a life-long career in it.

Also, I would like to thank all of my PhD dissertation committee members for their helpful advice, comments, and suggestions: Dr. Mark R. Matsumoto (Chemical and Environmental Engineering, UCR) and Dr. David Jassby (Chemical and Environmental Engineering, UCR). I would also like to thank Dr. Haizhou Liu (Chemical and Environmental Engineering, UCR) for his help and explanations. My sincere appreciation goes to our collaborators, Dr. Thanh Nguyen (University of Illinois, Urbana-Champaign) and her group for their invaluable support and accommodations when I was there several times.

Additionally, I am very grateful to numerous former and current post-doctorate/graduate student members from Dr. Walker's lab group, particularly Dr. Nichola Kinsinger, Dr. Indranil Chowdhury, Dr. Ian Marcus, Dr. Yongsuk Hong, Dr.

Gexin Chen, Dr. Hyun Jung “Nick” Kim, Dr. Berat Haznedaroglu, Dr. Amy Gong, Jacob Lanphere, Chen Chen, Jessamine Flores, and Alicia Taylor. I would like to also extend my thanks to graduate student researchers Lucy Liu and Michelle Bierman from Dr. Liu’s group for their assistance with some data collection. I would like to give my special thanks to the undergraduate researchers worked with me in my research including Tyler Abercrombie, Louise Daniels, Valerie Keene, Stacey Nwagbara, and Christine Brown.

Finally, I would like to thank my parents and my fiancé for their continuous support, enthusiasm, and motivation throughout my doctoral program.

This research was primarily supported by the National Science Foundation (NSF) Career Award (CBET 0954130). Additional sources of support were the Mentor Summer Research Internship Program (MSRIP) and NSF-supported Mentoring Year-Round Undergraduate Research (MY-BEST) at UCR.

Dedication

This PhD dissertation is dedicated to my parents and fiancé for their unceasing encouragement, inspiration, strength, patience, and love.

ABSTRACT OF THE DISSERTATION

Removal of Engineered Nanomaterials Through Conventional Water Treatment Processes

by

Ryan James Honda

Doctor of Philosophy, Graduate Program in Chemical and Environmental Engineering
University of California, Riverside, August 2014
Dr. Sharon L. Walker, Chairperson

The overall aim of this PhD research was to identify mechanisms involved in the removal of nanomaterials in conventional water treatment. This project was developed based upon the need for assessing current water treatment infrastructure, and its capacity of effectiveness in removing nanomaterials. The bulk of this dissertation investigated "primary treatment" steps of coagulation, flocculation, and sedimentation, simulated by full-scale and micro-scale jar tests. The remainder of the dissertation has been the development of a 2D micromodel flow cell to simulate the filtration stage. The model nanoparticles used in this research were primarily Degussa P25 titanium dioxide (TiO_2), with select experiments using meso-2,3-dimercaptosuccinic acid coated TiO_2, and fluorescently-labeled polystyrene latex microspheres.

Overall, >one-log removal was seen for the model groundwater for all coagulants at a constant dose of 50 mg/L, and across the range of particle concentrations tested (10, 25, 50, and 100 mg/L). In surface water, >90% removal was observed with $FeSO_4$ and $Al_2(SO_4)_3$, but <60% when using $FeCl_3$. Additionally, removal was most effective at

higher nanoparticle concentrations (50 and 100 mg/L) in AGW when compared to ASW. In the presence of more complex scenarios, results showed that removal was most efficient in the presence of divalent cations (Ca^{2+}), and in the absence of NOM and nanoparticle coating, achieving >1 log removal. However, with the presence of nanoparticle coating and NOM, removal decreased to a maximum of ~80%.

Finally, a 2D micromodel flow cell was designed and fabricated to demonstrate a new tool for the investigation of nanoparticle filtration. Specifically, the micromodel allows for direct visualization of pore-scale physico-chemical processes by using an array of 2D silica cylinders through which a model nanoparticle (i.e. fluorescent nanoparticles) can be transported. Through the development of this 2D system, future studies can compare filtration phenomena to a 3D macro-scale column experiment. Thus far, this study accomplished the following 1) fabrication of micromodels and construction of the experimental set-up, 2) development of a robust cleaning protocol for micromodel re-use, 3) demonstration of technique and confirmation that filtration trends (i.e. attachment efficiency) between our micromodel and published data from column experiments can be compared.

Table of Contents

List of Figures

List of Tables

Chapter 1

Introduction

1.1 Background and Motivation

With advancements in modern technology, the ability to design, fabricate, and produce materials at the nano-scale level is revolutionizing a new and innovative era of advanced materials that have the capacity for manufacturing devices, developing new techniques, and leading to new scientific breakthroughs. Nanomaterials are fundamentally changing and improving how various devices and materials are produced since they possess large surface-to-volume ratios, which gives them unique properties from their larger, bulk counterparts. The unique physic-chemical, electrical, and optical properties of nanomaterials have resulted in an increased usage in consumer products and industries[1], from which nanoparticles (NP) may be released into aquatic environments[2].

With the rapid growth in the nanotechnology industry, there has been an increase in production and consumption of nanomaterials in many common household products such as electronics, cosmetics, textiles, paints, and sunscreens[2,3,4,5]. The most commonly used nanomaterials for such applications include metal oxides (i.e. TiO_2, ZnO, Fe_XNi_{1-X}), core-based materials (i.e. CdTe, CdSe), and carbon-based materials (i.e. single and multi-walled carbon nanotubes, nanowires). However, with such high usages of nanomaterials, there is a growing concern on their toxicity, fate, transport, and removal of them in subsurface environments. With engineered nanomaterials being considered as a new class of environmental pollutants, current model paradigms and experimental techniques to determine the fate and removal of them must be sufficient enough to make sure that they can appropriately predict their distribution in the aquatic environments[6].

In recent studies, it has been shown that nanomaterials may be introduced into aquatic environments through various means such as product use, disposal, and recycling[2,7]. One example of a metal oxide nanomaterial that has been detected in biosolids and wastewater treatment effluent is titanium dioxide (TiO_2), which suggests that it may ultimately end up in the receiving water bodies[8,9], which is of high interests to water treatment practitioners. Exact levels of TiO_2 nanoparticles present in the environment are exactly not known due to limitations in current detection methods[10]. However, an approximate concentration of 0.180 – 1.230 mg/L of TiO_2 has been reported to be found in wastewater biosolids[8], and 0.01 – 3 mg/L in wastewater effluent[11]. Moreover, food grade nano-scale TiO_2 has a higher probability to enter sewage systems due to their high usage in consumer products. Each year, approximately 5,000 tons of nano-scale TiO2 is produced, with an expectation to continue increasing annually until 2025[3]. Within a decade's time, models have estimated that over 2 million tons of nano-scale TiO_2 will be produced[7]. Nano-scale TiO_2 has been previously reported to cause adverse health effects such as inducing oxidative stress in human cells[12] and genetic instabilities in mice[13]. For non-food grade TiO_2, they have the potential to enter waste streams through processes including industrial discharges or paint weathering, and may be introduced into the environment in the form of treated effluent discharge or biosolids that are applied to agricultural lands, incinerated wastes, or landfill solids[8]. Because of these possible phenomena for these emerging nanomaterial pollutants to enter and impact water supplies, it is vital to understand the movement of them in the aquatic environment, and to determine the most effective methods to remove them[14].

From a study by Keller *et al.* (2013)[9], an in-depth analysis of the global life cycle release of engineered nanomaterials showed their distribution through various environments. It was reported that 63–91% of about 300,000 metric tons of global ENM production in 2010 ended up in landfills, 8–28% in soils, 0.4–1.5% in water bodies, and 0.1– 1.5% into the atmosphere. They mentioned that TiO_2 was by far the most significant engineered nanomaterial released, in terms of exposure based on due to wide array of applications. In 2010, the estimated global production of TiO_2 was approximately 39,600 metric tons/year in coatings, paints and pigments, and about 30,800 metric tons/year in cosmetics. Additionally, the Keller study showed that waste water treatment plants (WWTPs) were an important intermediate pathway from the ENMs to soil and water. Approximately 17-34% of ENMs were likely to pass through WWTPs, which lead to 3-25% of releases into water bodies via treated effluent and 44-47% of emissions to soils via biosolids. Therefore, it is of critical importance that the mechanisms and behavior of TiO_2 are understood and identified in water treatment technologies.

Traditional water treatment plants utilize three primary stages coagulation, flocculation, and sedimentation (CFS) to remove particles. For the primary stages of treatment, chemical additives called coagulants – iron chloride ($FeCl_3$), iron sulfate ($FeSO_4$), and alum ($Al_2(SO_4)_3$) – help destabilize the particles in water suspensions at certain dosages, which are optimized depending on the solution chemistry (i.e. pH, water source type, concentration of pollutant) of the water[15,16,17]. Previous studies have demonstrated the use of conventional CFS water treatment processes to effectively remove natural organic matter, suspended solids, disinfection by-product precursors, and

other inorganic constituents from water and wastewater[18] but not at the nano-scale level of particles. The complete involvement of removal mechanisms in the destabilization and separation of nanomaterials is yet unknown. In addition, even with an extensive body of literature on these initial stages of water treatment and a growing number of papers on nanomaterial stability, the true capacity of these treatment stages to remove nano-sized particles has not yet been completed determined. Consequently, it is essential to understand and conduct a systematic study for the evaluation of current water treatment infrastructure in removing nanomaterials prior to them entering groundwater, surface water, and water distribution systems.

Research regarding the fate and transport of nanomaterials has been conducted extensively with the use of saturated and unsaturated columns to simulate soil environments. Studies have investigated nanomaterial transport and filtration processes of TiO_2[19,20,21,22] by utilizing a 3D macro-scale packed-bed columns. Though column experiments provide useful information on fate and transport – such as nanoparticle breakthrough, retention, and solution chemistry effects – understanding of the mechanistic phenomena such as attachment, deposition, straining, blocking, and other intermolecular forces at the pore-scale level is rather limited. Hence, to better understand such mechanisms in greater detail, the use of a 2D micromodel flow cell is necessary.

Micromodels allows for 2D pore-scale visualization of colloids through porous media, which simulate collector sand grains of a quartz packed-bed column. Previous work has been done to develop such micromodels[23,24,25,26]. A few studies have used

silicon fabricated micromodels to observe transport phenomena and attachment efficiencies of large (>1 μm) biological and colloid particles (non nano-sized particles)[24,27,28,29]. In those studies, real-time images were captured using a camera interfaced to a computer over a certain experimental duration of time, and were later evaluated for the mass transfer of particles to the collector surfaces. By being able to quantify number of particles attached on collector surfaces by counting, the single collector efficiency and attachment efficiency can be calculated. These parameters allow for a quantitative evaluation of the mechanistic behavior at the pore-scale level, which cannot be directly observed in a 3D macro-scale column.

Understanding the fate, transport, and removal of various nanoparticles in aquatic environments are of imperative concern. In typical water treatment plants, the primary stages of treatment (coagulation, flocculation, sedimentation) and filtration (granular media) have been known to remove biosolids and larger colloids (>500 μm) with 1-log removal efficiency or greater[30,15,16]. However, the primary stages of treatment were not initially designed for removal of nano-sized particles; thus, it is of critical importance that if nanomaterials are not removed effectively via the coagulation processes, filtration (i.e. transport through porous media) will need to be able to sufficiently remove them. While nanotechnology has great potential to improve and revolutionize water treatment technology, there is eminent concern regarding the introduction of nanomaterials in to the environment. Since nanomaterials possess unique properties and size, they may pose challenges in water treatment processes or other engineered systems since initial treatment infrastructure was not predicated on nano-sized particles. Therefore, this

doctoral research addresses such fundamental mechanisms and phenomena involving the removal of engineered nanoparticles through conventional water treatment processes in micro-scale systems.

1.2 Objective and Scope

The overall goal of this doctoral research was to investigate the fundamental mechanisms and phenomena governing the removal of engineered nanomaterials in both natural and engineered aquatic systems. Specifically, this study identified the capacity of traditional drinking water treatment processes to remove a model nanoparticle, TiO_2, and also investigate the attachment of latex nanoparticles in a fabricated micromodel to test the effectiveness of a filter. Specifically, the scope of this study involves simulation of the three primary stages of water treatment, which include coagulation, flocculation, and sedimentation (CFS); and filtration.

To evaluate the effectiveness of CFS, novel and systematic jar tests at the traditional (1 L) and reduced scale (100 mL) have been conducted to investigate this issue. The goals were to identify 1) how scaled-down version of jar tests could be used to evaluate the effectiveness of primary treatment and 2) what level of removal could be achieved under a range of representative environmental conditions. The first objective was to develop the scaled-down jar tests was to employ a system that achieved the same degree of removal as the conventional jar tests, while generating far less waste; notably, lower volumes of test solutions and amounts of nanoparticles (100 mg/L vs. 10 mg/0.1 L) were utilized. The second objective involved conducting tests under a range of relevant

solution chemistries and conditions. The parameters under consideration include coagulant dose and type, nanoparticle concentration, source water types (model groundwater and surface water), bare and DMSA-coated TiO_2 NP, and the presence or absence of natural organic matter (NOM) (i.e. Suwannee River Humic Acid) . Also, this work helped provide greater insight into the various mechanisms involved in particle removal. This study was designed to gain a greater understanding on nanomaterial removal mechanisms, and to evaluate each stage of primary treatment for nanoparticle removal capacity prior to subsequent filtration and distribution to domestic water supplies.

To evaluate the effectiveness of filtration, a 2D micromodel flow cell was developed and fabricated to investigate nanoparticle filtration. This method was selected to allow direct visualization of pore-scale physico-chemical processes by using an array of 2D silica cylinders through which a model nanoparticle (i.e. 20 nm fluorescent latex microspheres or fluorescently labeled engineered nanoparticles) can be transported. From the creation of this system, future studies can directly compare 2D micro-scale filtration phenomena to a 3D macro-scale packed-bed column experiment. This filtration study involved the 1) fabrication of silica micromodels in a cleanroom facility, 2) construction of a custom manifold assembly to properly accomodate the micromodel, 3) development of a cleaning protocol to allow for micromodel re-use, and 4) calculation of single collector efficiency for a model nanoparticle.

1.3 Organization of Dissertation

This entire PhD dissertation is composed of five chapters, including the Introduction section (Chapter 1) and Conclusion (Chapter 5). Following the Chapter 1 Introduction, Chapter 2 titled "Removal of TiO_2 nanoparticles during primary water treatment: Role of coagulant type, dose, and nanoparticle concentration," discusses the development of micro-scale jar tests determine the mechanisms involved in the removal of a model metal oxide nanoparticle, TiO_2, in artificial groundwater (AGW) and artificial surface water (ASW) at the primary stages of treatment: coagulation, flocculation, and sedimentation. Three different coagulants – iron chloride ($FeCl_3$), iron sulfate ($FeSO_4$), and alum ($Al_2(SO_4)_3$) – were used to destabilize the TiO_2 nanoparticles in both artificial source waters. Total particle removal was quantified at the end of each treatment stage by spectroscopy. Zeta potential was measured and compared between AGW and ASW with the presence of all three coagulants at the same treatment stage times as in the removal studies.

Chapter 3, entitled "Titanium Dioxide (TiO_2) Nanoparticle Removal: Role of Coating, Natural Organic Matter, Source Water, and Solution Chemistry" investigated how previously-scaled down jar tests remove bare and coated TiO_2 with a single coagulant, aluminum sulfate, to determine the fundamental mechanisms involved in removal in a simple monovalent electrolyte (KCl), more complex waters (artificial groundwater and surface water, and in the presence/absence of natural organic matter. Nanoarticle characterization measurements (zeta potential and hydrodynamic diameter)

were performed to link stability to removal. Results showed that removal was most efficient in the presence of divalent cations (Ca^{2+}) higher ionic strength, and in the absence of NOM and nanoparticle coating, achieving >1 log removal.

Chapter 4, titled "Development of a Micromodel Flow Cell for 2D Pore-scale Visualization of Filtration Processes" investigated how a 2D micromodel flow cell was designed, fabricated, and used as a means to investigate nanoparticle filtration mechanisms and phenomena. Essentially, this project was a proof-of-concept to observe the effectiveness of how a model nanoparticle (20 nm fluorescently-labeled latex microspheres) would transport and attach in a filter under a variety of different conditions. The effects of solution chemistry (i.e. pH, ionic strength, flowrate) were studied to see how transport and attachment were affected. Latex particles were quantified by capturing real-time images of deposition onto collector grain surfaces. Characterization studies were performed to determine the charge and size of latex nanoparticles under various conditions. Lastly, a systematic study involving micromodel cleaning and re-use possibility was conducted. These micromodel experiments have established a capacity in the laboratory to do more extensive filtration studies in the future.

Chapter 5, entitled "Summary and Conclusions" summarizes the findings from this PhD research. Some of the work in this dissertation has been published or submitted, while the most recent work (Chapter 4) provided a working proof-of-concept for later publications. Below is a list of manuscripts, which were a result from this research:

1. Honda, Ryan J., Keene, Valerie, Daniels, Louise, Walker, Sharon L. "Removal of TiO_2 Nanoparticles During Primary Water Treatment: Role of Coagulant Type, Dose, and Nanoparticle Concentration." *Environmental Engineering Science*. March 20, 2014. Vol. 31, No. 3: 127-134.
2. Honda, Ryan J., Keene, Valerie, Walker, Sharon L. "Titanium Dioxide (TiO_2) Nanoparticle Removal: Role of Coating, Natural Organic Matter, Source Water, and Solution Chemistry." Submitted June 2014, *Environmental Engineering Science*.

1.4 References

1. Nel, A.; Xia, T.; Mädler, L.; Li, N., Toxic Potential of Materials at the Nanolevel. *Science* **2006,** *311* (5761), 622-627.

2. Wiesner, M. R.; Lowry, G. V.; Alvarez, P.; Dionysiou, D.; Biswas, P., Assessing the Risks of Manufactured Nanomaterials. *Environ. Sci. Technol.* **2006,** *40* (14), 4336-4345.

3. Weir, A.; Westerhoff, P.; Fabricius, L.; Hristovski, K.; von Goetz, N., Titanium Dioxide Nanoparticles in Food and Personal Care Products. *Environ. Sci. Technol.* **2012,** *46* (4), 2242-2250.

4. Benn, T. M.; Westerhoff, P., Nanoparticle Silver Released into Water from Commercially Available Sock Fabrics. *Environmental Science & Technology* **2008,** *42* (11), 4133-4139.

5. Dunphy Guzmán, K. A.; Taylor, M. R.; Banfield, J. F., Environmental Risks of Nanotechnology: National Nanotechnology Initiative Funding, 2000−2004. *Environmental Science & Technology* **2006,** *40* (5), 1401-1407.

6. Westerhoff, P.; Nowack, B., Searching for Global Descriptors of Engineered Nanomaterial Fate and Transport in the Environment. *Acc. Chem. Res.* **2012,** *46* (3), 844-853.

7. Robichaud, C. O.; Uyar, A. E.; Darby, M. R.; Zucker, L. G.; Wiesner, M. R., Estimates of Upper Bounds and Trends in Nano-TiO2 Production As a Basis for Exposure Assessment. *Environ. Sci. Technol.* **2009,** *43* (12), 4227-4233.

8. Westerhoff, P.; Song, G.; Hristovski, K.; Kiser, M. A., Occurrence and removal of titanium at full scale wastewater treatment plants: implications for TiO2 nanomaterials. *J. Environ. Monit.* **2011,** *13* (5), 1195-203.

9. Keller, A.; McFerran, S.; Lazareva, A.; Suh, S., Global life cycle releases of engineered nanomaterials. *J. Nanopart. Res.* **2013,** *15* (6), 1-17.

10. Gottschalk, F.; Nowack, B., The release of engineered nanomaterials to the environment. *J. Environ. Monit.* **2011,** *13* (5), 1145-1155.

11. Kiser, M. A.; Westerhoff, P.; Benn, T.; Wang, Y.; Pérez-Rivera, J.; Hristovski, K., Titanium Nanomaterial Removal and Release from Wastewater Treatment Plants. *Environmental Science & Technology* **2009,** *43* (17), 6757-6763.

12. Long, T. C.; Saleh, N.; Tilton, R. D.; Lowry, G. V.; Veronesi, B., Titanium Dioxide (P25) Produces Reactive Oxygen Species in Immortalized Brain Microglia (BV2): Implications for Nanoparticle Neurotoxicity†. *Environ. Sci. Technol.* **2006,** *40* (14), 4346-4352.

13. Trouiller, B. R., R.; Westbrook, A.; Solaimani, P.; Schiestl, R.H., Titanium dioxide nanoparticles induce DNA damage and genetic instability in vivo in mice. *Cancer Res.* **2009,** *69* (22), 8784.

14. Zhang, Y.; Chen, Y.; Westerhoff, P.; Hristovski, K.; Crittenden, J. C., Stability of commercial metal oxide nanoparticles in water. *Water Res.* **2008,** *42* (8-9), 2204-12.

15. Crittenden, J. C.; Harza, M. W., *Water Treatment: Principles and Design*. Wiley: 2005.

16. Tchobanoglous, G.; Burton, F. L.; Stensel, H. D.; Metcalf; Eddy, I., *Wastewater Engineering: Treatment and Reuse*. McGraw-Hill Education: 2003.

17. Viessman, W., *Water Supply and Pollution Control*. Prentice Hall Higher Education: 2009.

18. Beltrán-Heredia, J.; Sánchez-Martín, J.; Solera-Hernández, C., Anionic Surfactants Removal by Natural Coagulant/Flocculant Products. *Ind. Eng. Chem. Res.* **2009,** *48* (10), 5085-5092.

19. Keller, A. A.; Wang, H.; Zhou, D.; Lenihan, H. S.; Cherr, G.; Cardinale, B. J.; Miller, R.; Ji, Z., Stability and Aggregation of Metal Oxide Nanoparticles in Natural Aqueous Matrices. *Environ. Sci. Technol.* **2010,** *44* (6), 1962-1967.

20. Chowdhury, I.; Hong, Y.; Honda, R. J.; Walker, S. L., Mechanisms of TiO2 nanoparticle transport in porous media: Role of solution chemistry, nanoparticle concentration, and flowrate. *J. Colloid Interface Sci.* **2011,** *360* (2), 548-555.

21. Joo, S. H.; Al-Abed, S. R.; Luxton, T., Influence of Carboxymethyl Cellulose for the Transport of Titanium Dioxide Nanoparticles in Clean Silica and Mineral-Coated Sands. *Environmental Science & Technology* **2009,** *43* (13), 4954-4959.

22. Dunphy Guzman, K. A.; Finnegan, M. P.; Banfield, J. F., Influence of Surface Potential on Aggregation and Transport of Titania Nanoparticles. *Environ. Sci. Technol.* **2006,** *40* (24), 7688-7693.

23. Baumann, T.; Werth, C. J., Visualization and Modeling of Polystyrol Colloid Transport in a Silicon Micromodel. *Vadose Zone J.* **2004,** *3* (2), 434-443.

24. Auset, M.; Keller, A. A., Pore-scale visualization of colloid straining and filtration in saturated porous media using micromodels. *Water Resources Research* **2006,** *42* (12), W12S02.

25. Keller, A. A.; Auset, M., A review of visualization techniques of biocolloid transport processes at the pore scale under saturated and unsaturated conditions. *Advances in Water Resources* **2007,** *30* (6–7), 1392-1407.

26. Willingham, T. W.; Werth, C. J.; Valocchi, A. J., Evaluation of the Effects of Porous Media Structure on Mixing-Controlled Reactions Using Pore-Scale Modeling and Micromodel Experiments. *Environmental Science & Technology* **2008,** *42* (9), 3185-3193.

27. Liu, Y.; Zhang, C.; Hilpert, M.; Kuhlenschmidt, M. S.; Kuhlenschmidt, T. B.; Nguyen, T. H., Transport of Cryptosporidium parvum Oocysts in a Silicon Micromodel. *Environmental Science & Technology* **2012,** *46* (3), 1471-1479.

28. Liu, Y.; Zhang, C.; Hu, D.; Kuhlenschmidt, M. S.; Kuhlenschmidt, T. B.; Mylon, S. E.; Kong, R.; Bhargava, R.; Nguyen, T. H., Role of Collector Alternating Charged Patches on Transport of Cryptosporidium parvum Oocysts in a Patchwise Charged Heterogeneous Micromodel. *Environmental Science & Technology* **2013,** *47* (6), 2670-2678.

29. Lu, N.; Bevard, T.; Massoudieh, A.; Zhang, C.; Dohnalkova, A. C.; Zilles, J. L.; Nguyen, T. H., Flagella-Mediated Differences in Deposition Dynamics for Azotobacter vinelandii in Porous Media. *Environmental Science & Technology* **2013,** *47* (10), 5162-5170.

30. Gregory, J., *Particles in Water: Properties and Processes*. Taylor & Francis: 2005.

Chapter 2

Removal of TiO_2 nanoparticles during primary water treatment: Role of coagulant type, dose, and nanoparticle concentration

Reprinted with permission from ENVIRONMENTAL ENGINEERING SCIENCE, Volume 31, No. 3, 2014, published by Mary Ann Liebert, Inc,. New Rochelle, NY

Honda, Ryan J., Keene, Valerie, Daniels, Louise, Walker, Sharon L. "Removal of TiO_2 Nanoparticles During Primary Water Treatment: Role of Coagulant Type, Dose, and Nanoparticle Concentration." *Environmental Engineering Science*. March 20, 2014. Vol. 31, No. 3: 127-134.

Abstract

Nanomaterials from consumer products (i.e. paints, sunscreens, toothpastes, and food-grade TiO_2 have the capacity to end up in groundwater and surface water, which is of high concern since the effectiveness of removing them via traditional treatment is relatively uncertain. Although aggregation and transport of nanomaterials have been investigated, studies on its removal from suspension are limited. Hence, this study involves the development of scaled-down jar tests to determine the mechanisms involved in the removal of a model metal oxide nanoparticle, TiO_2, in artificial groundwater (AGW) and artificial surface water (ASW) at the primary stages of treatment: coagulation, flocculation, and sedimentation. Total removal was quantified at the end of each treatment stage by spectroscopy. Three different coagulants – iron chloride ($FeCl_3$), iron sulfate ($FeSO_4$), and alum ($Al_2(SO_4)_3$) – destabilized the TiO_2 nanoparticles in both source waters. Overall, >one-log removal was seen in groundwater for all coagulants at a constant dose of 50 mg/L and across the range of particle concentrations (10, 25, 50, and 100 mg/L). In surface water, >90% removal was seen with $FeSO_4$ and $Al_2(SO_4)_3$, but <60% when using $FeCl_3$. Additionally, removal was most effective at higher nanoparticle concentrations (50 and 100 mg/L) in AGW when compared to ASW. Zeta potential was measured and compared between AGW and ASW with the presence of all three coagulants at the same treatment stage times as in the removal studies. These electrokinetic trends confirm that the greatest total removal of nanoparticles occurred when the magnitude of charge was smallest (< 10 mV) and conversely, higher zeta potentials values (> 35 mV) measured were under conditions with poor removal (< 90%).

These results are anticipated to be of considerable interest to practitioners for the assessment of traditional treatment processes' capacity to remove nanomaterials prior to subsequent filtration and distribution to domestic water supplies.

2.1 Introduction

The unique physicochemical, optical, and electrical properties of nanomaterials have resulted in an increased usage in consumer products and industries (Nel, Xia et al. 2006), from which nanoparticles (NP) may be released into aquatic environments (Wiesner, Lowry et al. 2006). The rapid growth of the nanotechnology industry has led to increased production and consumption of nanomaterials in common household products such as cosmetics, paints, and sunscreens (Weir, Westerhoff et al. 2012). Recent studies have shown that nanomaterials can be introduced into the aquatic environment via product use, disposal, and recycling (Wiesner, Lowry et al. 2006; Robichaud, Uyar et al. 2009). One nanomaterial that has been detected in biosolids and wastewater treatment effluent is titanium dioxide (TiO_2), suggesting it may ultimately end up in the receiving water bodies (Westerhoff, Song et al. 2011; Keller, McFerran et al. 2013). Exact levels of TiO_2 nanoparticles present in the environment are not known due to limitations in current detection methods (Gottschalk and Nowack 2011). However, an approximate concentration between 0.180 – 1.230 mg/L has been reported as levels found in wastewater biosolids (Westerhoff, Song et al. 2011).

Additionally, food grade nanoscale TiO_2 has a higher probability to enter sewage

systems due to their frequent presence in personal care products, toothpastes, candies, and chewing gum (Weir, Westerhoff et al. 2012). About 5,000 tons of nanoscale TiO_2 are produced annually, and is expected to increase annually until 2025 (Weir, Westerhoff et al. 2012). Non-nano based TiO_2 production in industries are predicted to be converted into nano-based TiO_2 where the nano-scale levels will rise from about 200,000 tons in year 2014 to 2.5 million tons by year 2025 (Robichaud, Uyar et al. 2009). Non-food grade TiO_2 may also make it into waste streams through such mechanisms as paint weathering or industrial discharges. Subsequently, they may be introduced into the environment in the form of treated effluent discharge or biosolids applied to agricultural lands, incinerated wastes, or landfill solids (Zhang, Chen et al. 2008; French, Jacobson et al. 2009). As such, NP are considered emerging pollutants that have the capacity to enter and impact water supplies. Thus, it is of critical importance to understand the movement of nanomaterials (Domingos, Tufenkji et al. 2009) in various model aquatic environments (Zhang, Chen et al. 2008) and determine how they can be most effectively removed through conventional water treatment processes. This is of concern since nanoscale TiO_2 have been reported to cause adverse effects such as oxidative stress in human cells (Long, Saleh et al. 2006; Xia, Kovochich et al. 2008) and genetic instabilities in mice (Trouiller 2009).

Metal oxide nanoparticle aggregation in water is a well-known phenomenon. Various groups have demonstrated nanoparticle aggregation through a combination of stability tests and transport studies (Zhang, Chen et al. 2008; French, Jacobson et al. 2009; Keller, Wang et al. 2010; Chowdhury, Hong et al. 2011). These studies have

shown that aggregation is a significant mechanism governing nanoparticle behavior and provides insight into how they may be transported or removed in the environment. Such that observed trends in this current study can be evaluated, the fundamental mechanisms involved in particle separation are described briefly here. It is common to refer to coagulation as the destabilization step, which is induced by the introduction of polymers or salts. Flocculation refers to cases where polymer bridging dominates through fluid motion (i.e. orthokinetic aggregation) and aggregates (flocs) tend to be larger (Benjamin 2002; Gregory 2005). It has been reported that metal salts (i.e. aluminum, iron) are effective in removing colloidal particles and dissolved organic substances through charge neutralization and sweep flocculation mechanisms (Duan and Gregory 2003). Specifically, the Duan and Gregory (2003) study found that charge neutralization can be effective in destabilizing colloidal particles at low dosages of aluminum and ferric salts (5 – 50 μM), bulk precipitation of metal hydroxide yielded larger flocs from sweep flocculation, and that optimum pH is important for the effectiveness of the coagulant. Sweep flocculation leads to faster aggregation than charge neutralization, and gives stronger/denser flocs (Gregory 2005). Moreover, an important phenomena involving the effectiveness of metal coagulants is from the pH change caused by hydrolysis of the metal cations (in this case, Al^{3+} and Fe^{3+}); the change in pH of the solution governs the metal coagulants' effectiveness during coagulation since metal ion solubility will be affected (Crittenden and Harza 2005; Gregory 2005). Others have demonstrated the use of conventional water treatment processes (i.e. coagulation, flocculation, sedimentation) to effectively remove natural organic matter, suspended solids, disinfection by-product

precursors, and other inorganic constituents from water and wastewater (Duan, Wang et al. 2002; Domínguez, Beltrán de Heredia et al. 2005; Beltrán-Heredia, Sánchez-Martín et al. 2009; Zhao, Liu et al. 2009; Kim, Liu et al. 2012). However, even with these studies and many others, the involvement of these removal mechanisms in the destabilization and separation of nanomaterials is yet unknown. Furthermore, even with an extensive body of literature on these initial stages of water treatment and a growing number of papers on nanomaterial stability, the capacity of these treatment stages to remove nanomaterials has not yet been fully determined. Thus, it is imperative to conduct a systematic study for the assessment of current water treatment infrastructure in removing nanomaterials prior to their entering water distribution systems, groundwater, and surface waters (Lecoanet and Wiesner 2004; Dunphy Guzman, Finnegan et al. 2006).

The overall aim of this research is to identify the capacity of traditional drinking water treatment processes to remove a model nanoparticle (TiO_2). Specifically, the scope of this study involves simulation of the three primary stages of water treatment, which include coagulation, flocculation, and sedimentation. While current infrastructure technology has been designed to generally remove particles during water treatment, no study has been done specifically addressing the removal of nanomaterials in these processes. Therefore, systematic jar tests at the traditional (1 L) and reduced scale (100 mL) have been conducted to investigate this issue. The goals are to identify 1) whether a scaled-down version of jar tests could be used to evaluate the effectiveness of primary treatment and 2) what level of removal could be achieved under a range of representative conditions. The objective of developing the scaled-down jar tests is to employ a system

that achieves the same degree of removal as the conventional jar tests, while generating far less waste; notably, lower volumes of test solutions (1 L vs. 0.1 L) and amounts of nanoparticles (100 mg/L vs. 10 mg/0.1 L) are utilized. The second objective involves conducting tests under a range of relevant solution chemistries and conditions. The parameters under consideration include coagulant dose and type, nanoparticle concentration, source water types (model groundwater and surface water), and general operating conditions. The objective is to evaluate each stage of primary treatment for nanoparticle removal capacity prior to subsequent filtration and distribution to domestic water supplies.

2.2 Experimental Protocols

2.2.1 TiO_2 Nanoparticles

The TiO_2 nanoparticles used in this study were Evonik Degussa P25 TiO_2 nanoparticles, which are an industrial grade TiO_2 with a structural composition of 82% rutile and 18% anatase. According to the manufacturer, the nanoparticles were greater than 99.5% pure and have a primary particle size of ~20 nm. Previous work with transmission electron microscopy has verified a similar effective diameter of TiO_2 to be ~18 ± 6.0 nm (Chowdhury, Hong et al. 2011), which is similar to the manufacturer's reported average particle size. Prior to all experiments, a stock suspension of TiO_2 nanoparticles was prepared by a previously reported protocol (Chowdhury, Hong et al. 2011) involving two minutes of sonication (Transsonic 460/H, Barnstead/Lab-line, Melrose Park, IL) in the background solution. Nano-TiO_2 was selected as the model

engineered nanoparticle as it will be one of the most common nanomaterials prevalent in the aquatic environment (Keller, McFerran et al. 2013). Bulk-sized TiO_2 was not used as the particles selected for this study were effectively micron-sized aggregates based on the solution conditions tested. Additionally, increased reactivity of nanoparticles, despite aggregate sizes compared to bulk-sized TiO_2, has been shown. Studies have demonstrated that the band gap of TiO_2 changed as a function of primary particle size (< 20 nm) (Lin, Huang et al. 2006).

2.2.2 Test Solutions

The two test solutions used in this study were artificial groundwater (AGW) (Bolster, Mills et al. 1999) and artificial surface water (ASW) (Yip, Tiraferri et al. 2011) to simulate environmentally-relevant source waters typically entering water treatment plants. The ionic strength of the two solutions was 0.01 M and 0.00183 M for AGW and ASW, respectively. The total salt concentration in AGW is 630.9 mg/L and is comprised of six different salts: $CaCl_2 \cdot 2H_2O$, $CaSO_4 \cdot 2H_2O$, KNO_3, $NaHCO_3$, $Ca(NO_3)_2 \cdot 4H_2O$, and $MgSO_4 \cdot 7H_2O$. ASW has a total salt concentration of 80.1 mg/L that is eight times less in mass concentration than AGW, and it is composed of: $MgCl_2 \cdot 6H_2O$, $MgSO_4$, $KHCO_3$, $NaHCO_3$, and $CaCO_3$. All chemicals used were either ACS grade reagents (purchased from Fisher Scientific, Fair Lawn, New Jersey) or research grade (from Mallinckrodt Chemical, Japan; and Acros Organics, New Jersey).

2.2.3 Jar Test Experiments

The first primary treatment stage in water treatment is coagulation. Coagulation, also known as a rapid or "flash" mixing process, refers to the step where anionic or cationic polymers are added into the water in an effort to destabilize suspended material (Bratby 2006). Typical operating parameters for coagulation involves 150 - 300 rpm mixing for 1 - 2 minutes (Crittenden and Harza 2005; Bratby 2006). Next is flocculation, where the destabilized particles and primary flocs collide and agglomerate to a size and density that will readily settle to the bottom (Bratby 2006). This process is facilitated by slow mixing, typically 25 - 40 rpm mixing on the order of 30 minutes (Spellman and Drinan 2000; Crittenden and Harza 2005). Finally, sedimentation, also known as clarification, involves gravity-induced settling of the resulting floc, remaining particulate matter, and precipitates from suspension in the absence of any mixing over 1 to 4 hours (Spellman and Drinan 2000; Crittenden and Harza 2005)

Two scales of jar test analyses were conducted, at the conventional (1 L) and a novel "scaled-down" (100 mL). The operating parameters, which include the mixing speeds and length of three critical treatment steps – coagulation, flocculation, and sedimentation (CFS) – were set based on values reported from actual CFS stages in water treatment plants (Crittenden and Harza 2005). To simulate flash mixing, both the conventional and scaled-down jar tests employed maximum feasible mixing speeds (300 rpm for conventional jar tests and 150 rpm for the scaled-down version) and lasted for one minute. Prior to the start of experimentation (i.e. before the coagulation process), the

TiO_2 suspension was sonicated and stirred. The equilibration time for the jar test experiments were as follows: (1) after sonication of the TiO_2, there is approximately a two minute interval for dispensing the nanoparticle solution (while stirring) into the four 100 mL jars prior to coagulant addition; (2) then, the coagulant was pipetted immediately (~two sec.) prior to turning on the mixer. Flocculation was conducted 30 rpm for both cases that lasted for 30 minutes. Finally, a one hour non-mixing sedimentation stage was implemented. The conventional jar tests were performed with a traditional apparatus of six vertical paddle stirrers (Philips and Bird Unit of General Medical Corp, Richmond, VA). The scaled-down jar test was conducted using a stir plate with four, simultaneously spinning magnets (Corning Laboratory Systems, United Kingdom) and FDA-grade octagonal magnetic stir bars that measure 2.54 cm in length and 0.79 cm in diameter (Fisher Scientific).

Three different coagulants were used in this study: iron chloride ($FeCl_3$), iron sulfate ($FeSO_4$), and alum ($Al_2(SO_4)_3$). These are commonly used choices in industry (Tchobanoglous, Burton et al. 2003), most notably iron chloride and alum. The TiO_2 concentration was 100 mg/L for all experiments, with the exception for the experiments investigating the role of TiO_2 concentration on removal. Experiments were conducted in both AGW and ASW at nanoparticle concentrations of 10, 25, 50, and 100 mg/L. The concentration of nanoparticles was selected to be artificially high such that their concentration could be measured in the spectrophotometer when removal levels of > 90% are achieved. The influence of coagulant dose was investigated in AGW with the three

coagulants at 30, 40, 50, and 60 mg/L, which are representative of a range commonly used in industry (Tchobanoglous, Burton et al. 2003; Crittenden and Harza 2005).

Jar test experimentation consisted of three coagulants at a constant dosage of 50 mg/L each and nanoparticle concentration of 100 mg/L in AGW and ASW. 1.5 mL samples were drawn from the center point and ~ 1 mm depth in the beakers at the end of the three treatment stages for both the scaled-down and full-scale jar tests. Sampling times of 0, 30, and 90 minutes correspond to the end of the following three stages of treatment at which absorbance was read: at 1 min for flash mix, 30 min of flocculation, and 1 hr of sedimentation. The samples were measured in a spectrophotometer (DU 800 Beckman Coulter, Fullerton, CA) at a wavelength of 370 nm. This value was determined using the automatic time-scan feature on the spectrophotometer to determine the optimum wavelength for measuring TiO_2. Despite the lack of a distinct peak, TiO_2 does strongly absorb light smaller than 400 nm (band gap energy of 3.0 eV) (Linsebigler, Lu et al. 1995; Lin, Huang et al. 2006; Palominos, Mora et al. 2008) proportionally to the mass concentration of the suspension. There have also been other studies that have successfully employed this technique of using a UV-Vis to measure relative concentration of nanoparticles (Keller, Wang et al. 2010; Dalai, Pakrashi et al. 2012).

Total particle removal was evaluated at each of the three stages of treatment (coagulation, flocculation, and sedimentation). The results are plotted as $1 - A/A_0$ versus time, when A/A_0 is the ratio of measured absorbance over the initial absorbance (initial refers to the experiment at time “0 min” before the addition of coagulant) and time

accounts for the minutes elapsed since the nanoparticles were added to the solution. The expression $1 - A/A_0$ is expressed as a percentage and represents the total particle removal from the start of the jar test through each phase of treatment.

2.2.4 Characterization

Electrokinetic characterization (zeta potential) was conducted using a ZetaPALS analyzer (Brookhaven Instruments Corp., Holtsville, NY) and measurements were taken immediately after each of the three treatment processes – coagulation, flocculation, and sedimentation – were complete. Hydrodynamic diameter was measured using dynamic light scattering (DLS) (Brookhaven model BI-9000AT, Holtsville, NY) at the end of each of the three treatment stages. Both the zeta potential and hydrodynamic diameters were determined from the arithmetic average of five runs with each run lasting two minutes. Each measurement required ~2 mL of test sample for both zeta potential and DLS.

2.3 Results and Discussion

2.3.1 Conventional vs. Scaled-down Jar Tests

Validation of the use of the scaled-down jar tests (100 mL vs. conventional 1 L jars) was conducted to ensure that the smaller scale experiments achieved the same degree of removal as in traditional jar tests. The results of these comparison tests are presented in Figure 2.1.

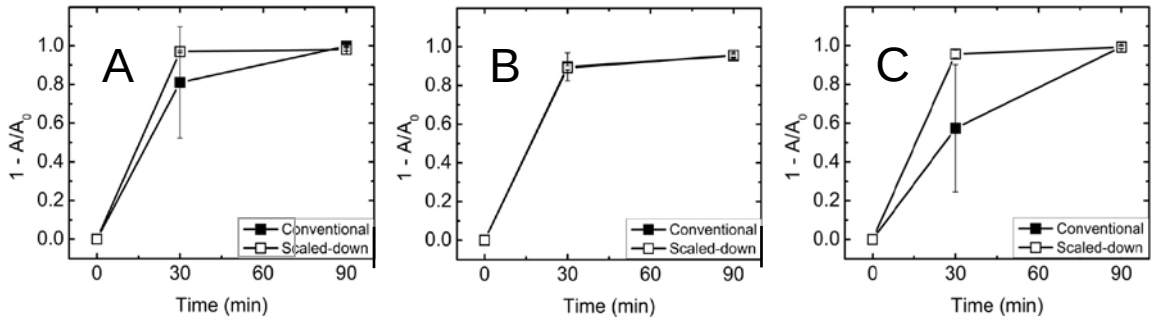

Figure 2.1. Conventional vs. micro-scale jar tests were evaluated as a function of total particle removal ($1 - A/A_0$) over time in AGW. Times 0, 30, and 90 minutes correspond to the end of the following three stages of treatment: a one minute flash mix, 30 min of flocculation, and 1hr of sedimentation. The three coagulants used were $FeCl_3$ (A) $FeSO_4$ (B) and alum (C) at dosage of 50 mg/L. TNP concentration was 100 mg/L. Operating parameters were: 150 rpm coagulation for 1 minute, 30 rpm flocculation for 30 minutes, and 0 rpm sedimentation for 60 minutes.

As seen from Figure 2.1, approximately 95-100% removal was reached over the entire course of the experiments (as judged by the total particle removal achieved at 90 minutes, the end of the sedimentation phase). This removal level occurs regardless of coagulant type or scale of system (conventional or scaled-down). For example, the total particle removal achieved subsequent to sedimentation with coagulant $FeCl_3$ and alum remained at combined (both scales) average removal of 99.7%±0.1% and 99.4%±1.0% , respectively, and the differences between the two scales were statistically insignificant ($P = 0.41$) as verified by an ANOVA test run in Microsoft Excel (v. 2007). Removal in the presence of iron sulfate was a bit lower than the other two coagulants, at about 95.3% ± 0.8% effective. The only notable differences occurred during the flocculation stage, where the total removal from across the three stages to greater than 80% in all cases, except in the conventional scale with alum (<60%). However, by the end of the

sedimentation phase of treatment the total particle removal achieved was effectively the same. These experiments demonstrated the capacity for the scaled-down (100 mL) jar tests to simulate the conventional (1 L) apparatuses ones; hence, all subsequent jar tests discussed herein are those conducted in the scaled-down system.

2.3.2 Role of Coagulant Type and Dosage

The relative effectiveness of three commonly used coagulants – iron chloride ($FeCl_3$), iron sulfate ($FeSO_4$), and alum ($Al_2(SO_4)_3$) – was compared over a range of doses in AGW. These results are presented in Figure 2.2.

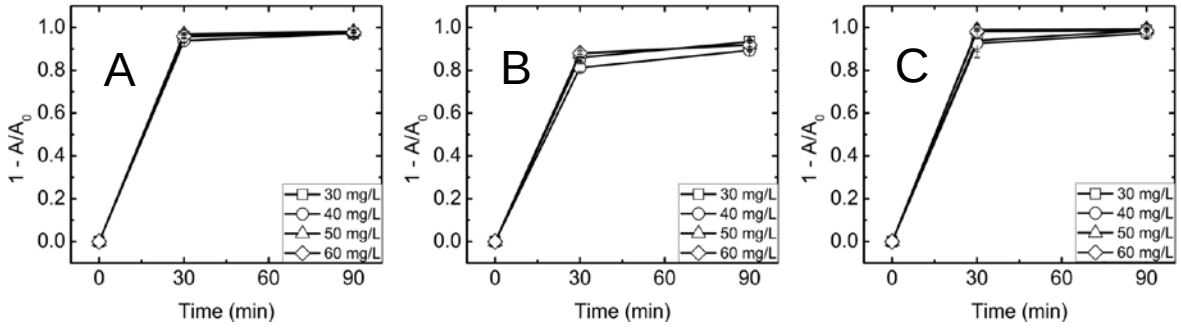

Figure 2.2. The total TiO_2 removal was plotted as a function of coagulant dose in AGW in the micro-scale jar tests over time with the three coagulants using four different dosages: 30, 40, 50, and 60 mg/L. TiO_2 concentration remained constant in all experiments at 100 mg/L. The three coagulants used were $FeCl_3$, $FeSO_4$, and alum at dosage of 50 mg/L. Operating parameters were: 150 rpm coagulation for 1 minute, 30 rpm flocculation for 30 minutes, and 0 rpm sedimentation for 60 minutes.

The removal trends are quite similar between the three coagulants across all doses tested, with the greatest removal occurring during the coagulation and flocculation stage. Notably, 90% of the total removal in all cases occurred in these first 30 minutes of

treatment. $FeCl_3$ and $Al_2(SO_4)_3$ performed the best, achieving an average removal of 97.5%±2.0% and 98.0%±2.8%, respectively, as compared to a lower value of 92.0%±1.8% for $FeSO_4$. The difference in removal when using $FeCl_3$ and $Al_2(SO_4)_3$ was statistically insignificant ($P = 0.11$).

Coagulant doses below 50 mg/L yielded poorer removal levels, indicating a higher dose coagulant was required. An experiment conducted at 30 mg/L of coagulant dose yielded lower removal when compared to increased dosages (>30 mg/L), except at 60 mg/L. Above 50 mg/L, there was an excess of coagulant, causing additional turbidity of the water due to an increased amount of particles present in the suspension, which subsequently increases the absorbance value reading. This performance was optimized based on a NP concentration of 100 mg/L. As such, the subsequent experiments were conducted at the selected coagulant dose of 50 mg/L. In contrast, experiments in the absence of coagulants were also conducted to demonstrate TiO_2 removal with no chemical aid. Results showed that the total particle removal after sedimentation was 71.5%±4.89% in AGW and 69.5%±1.91% in ASW, respectively.

2.3.3 Role of TiO_2 Nanoparticle Concentration

The contribution of nanoparticle concentration to total removal during treatment, tested in both AGW and ASW with a constant coagulant dose of 50 mg/L, is reported in Figures 2.3 and 2.4, respectively. Figure 2.3 presents the total removal data with $FeCl_3$ (3A) with $FeSO_4$ (3B) and with $Al_2(SO_4)_3$ (3C).

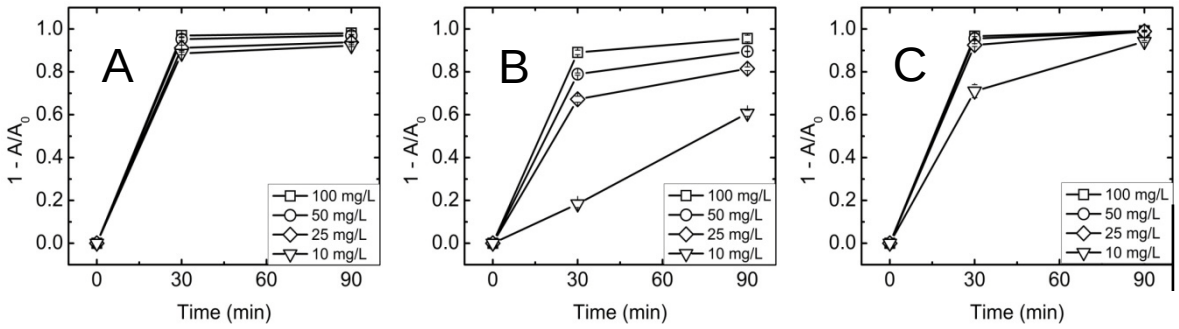

Figure 2.3. Total TiO_2 removal was plotted as a function nanoparticle concentration in AGW in the micro-scale jar tests. The TiO_2 concentrations ranged from 10, 25, 50, and 100 mg/L. The three coagulants used were $FeCl_3$ (A), $FeSO_4$ (B), and alum (C). Coagulant dose remained constant at 50 mg/L with all three coagulants for all experiments. Operating parameters were: 150 rpm coagulation for 1 minute, 30 rpm flocculation for 30 minutes, and 0 rpm sedimentation for 60 minutes.

$FeCl_3$ and $Al_2(SO_4)_3$ resulted in similar trends in AGW with an average total particle removal of 95.2%±0.4% with $FeCl_3$ and 97.4%±0.6% with alum after sedimentation for the four TiO_2 concentrations. In $FeSO_4$, the removal was similar to the other coagulants at 100mg/L TiO_2 (94.2%±0.6%), but was notably lower removal at nanoparticle concentrations <100mg/L (60.7%±1.4%, 81.5%±0.9%, and 89.6%±0.1% total removal at 10, 25, and 50 mg/L, respectively). Poorer removal of the nanoparticles occurs at the lower concentrations (particularly at 10 mg/L) due to insufficient collisions occurring between particles during the mixing stages. This indicates that the presence of a coagulant aid such as bentonite clay particles is needed (Yang, Tong et al. 2012), as the coagulant aid can induce a higher collision frequency between the coagulant and nanoparticle and, thus, improve aggregation between particles (Kim, Liu et al. 2012).

The trends described above are observed in the artificial surface water as well.

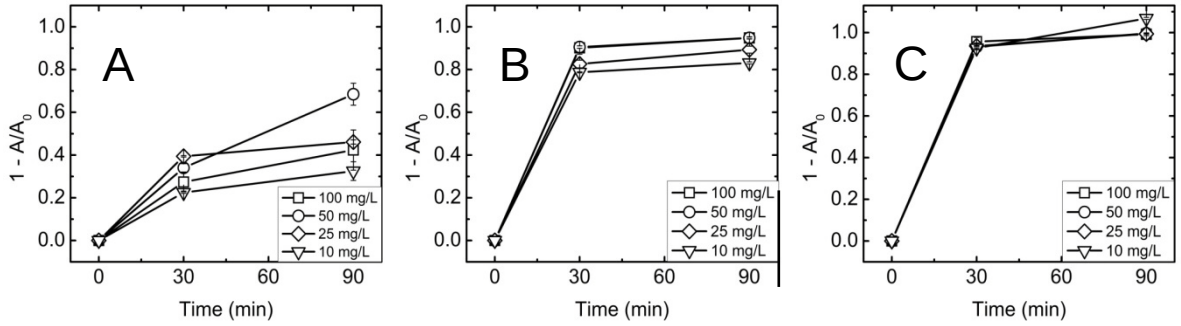

Figure 2.4. Total TiO_2 removal was plotted as a function nanoparticle concentration in ASW in the micro-scale jar tests. The TiO_2 concentrations tested were 10, 25, 50, and 100 mg/L. The three coagulants used were $FeCl_3$ (A), $FeSO_4$ (B), and alum (C). Coagulant dose remained constant at 50 mg/L with all three coagulants for all experiments. Operating parameters were: 150 rpm coagulation for 1 minute, 30 rpm flocculation for 30 minutes, and 0 rpm sedimentation for 60 minutes.

Figure 2.4B and 2.4C displays similar total particle removal trends with $FeSO_4$ achieving about a 91.8%±1.7% effectiveness and alum nearly 100%±0.6% after sedimentation across all four TiO_2 concentrations in ASW. However, $FeCl_3$ resulted in much poorer removal levels (Figure 2.4A), with removal dropping off nearly to two times less than that of $FeSO_4$ and alum. The total particle removal at 10, 25, 50, and 100 mg/L TiO_2 when using $FeCl_3$ was 32.5%±4.4%, 46.2%±1.0%, 68.5%±5.1%, and 47.9%±21.7%, respectively. Clearly, there is a notable difference in removal capacity with $FeCl_3$ when comparing the two source waters (95% effective in AGW; only 48% in ASW). Out of the three coagulants tested, $FeCl_3$ demonstrated the most consistent removal of TiO_2 at high concentrations of 50 and 100 mg/L, regardless of solution chemistry (water type)

and particle concentration. This is further confirmation that the coagulant type and dose must be selected for the water source at a particular site.

2.3.4 Characterization of TiO_2 Nanoparticles

Extensive electrokinetic characterization of the nanoparticles was conducted in an effort to mechanistically explain the results of the jar tests. Outcomes of this characterization are reported in Figure 2.5.

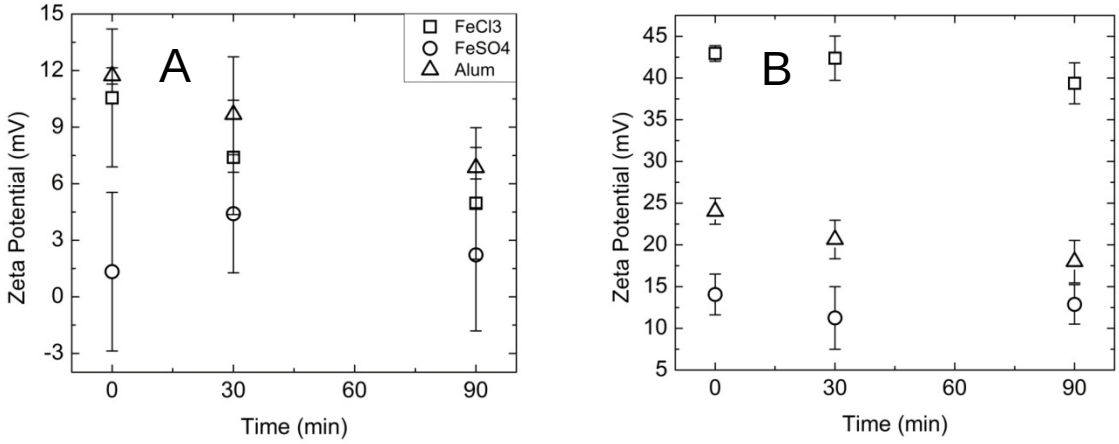

Figure 2.5. Zeta potential (mV) measurements of TiO_2 for each of the three coagulants in both AGW (A) and ASW (B) measured over the course of the jar tests. Times 0, 30, and 90 minutes correspond to the end of the following three stages of treatment: a one minute flash mix, 30 min of flocculation, and 1hr of sedimentation. Zeta potential ranged between 0-12 mV in AGW and 10-45 mV in ASW. The pH of AGW was 8.01 and 9.4 for ASW.

The TiO_2 nanoparticles became less negatively charged across the range of aquatic parameters tested as the pH values became more acidic with the addition of coagulant (albeit the pH was still above the isoelectric point for TiO_2) (Chen and Li 2010). As expected, the zeta potential (Figure 2.5) was observed to be sensitive to the type of water

and coagulant used. The sensitivity to water source is linked to the pH of the two model solutions, which was found to be 9.4 and ~8 for ASW and AGW, respectively. With the addition of each coagulant, the pH of the two model waters was reduced even further. The most notable impact on pH was seen with $FeCl_3$, where the pH dropped almost six log units to 3.9 in ASW. The pH of the water, in addition to the ionic content, impacted the subsequent electrokinetic properties of the nanoparticles. Stability of the nanoparticles is affected by pH changes since TiO_2 will interact with other particles based on its isoelectric point (~6.2). The pH of AGW was approximately 8 and became more acidic with the addition of coagulant (pH 6.56, 7.58, and 7.42 for $FeCl_3$, $FeSO_4$, and $(Al_2(SO_4)_3$, respectively). As seen from the zeta potential data for particles in AGW (Figure 5A), even with this change in pH, the relative magnitude of zeta potentials were similar between all three coagulants. After sedimentation, the zeta potential values for $FeCl_3$, $FeSO_4$, and $(Al_2(SO_4)_3$ were 5.0±3.0, 1.6±4.9, and 6.8±2.1, respectively. These values directly correspond to the removal data trends as seen in Figure 2.3 with an average of about 90% removal in all cases, except with $FeSO_4$ at 10 mg/L TiO_2 concentration. When comparing the zeta potential and removal data, a correlation between removal and zeta potential is seen (with removal decreasing with more substantial zeta potential values). pH clearly impacts the results because TiO_2 normally has a point of zero charge at a pH of about 6.2 under similar conditions (Chowdhury, Hong et al. 2011). In this study, the pH of AGW was ~8 and the addition of the coagulant made the solution more acidic. The lower zeta potential value indicates that the nanoparticles were less stable and, therefore, more effectively removed during the jar

test. Hence, the selection of coagulant impacted the removal efficiency due to the coagulants influence of solution chemistry and subsequent particle charge, which is consistent with other studies looking at the removal of organic matter, turbidity, and metal oxides (Domínguez, Beltrán de Heredia et al. 2005; Morfesis, Jacobson et al. 2008; Zhang, Chen et al. 2008; Yu, Gregory et al. 2010).

In contrast, zeta potential values for nanoparticles in ASW had dissimilar results between the three coagulants as seen in Figure 2.5B. The pH of ASW is ~9.4 and becomes more acidic when each of the three coagulants was added (3.92, 7.23, and 7.21 for $FeCl_3$, $FeSO_4$, and alum, respectively). pH was not controlled in the experiments to determine the coagulants' effectiveness in solutions simulating "natural" water sources – especially as groundwater and surface water are mildly basic by nature (Winter 1999; Crittenden and Harza 2005). The zeta potential of the nanoparticles in ASW ranged from 42.4±2.5, 12.9±2.4, and 18±2.5 mV in the presence of $FeCl_3$, $FeSO_4$, and alum, respectively. This data helps explain the poor removal phenomena with $FeCl_3$ from Figure 4, as the larger zeta potential indicates greater stability and reduced capacity for the particles to aggregate and be removed by gravitational sedimentation.

Zeta potential measurements provide insight into the particle stability as the greater the magnitude of the zeta potential, the higher the particle stability. In general, the zeta potential trends agree with the total removal data as presented in Figure 2.4. For example, total particle removal was the lowest in ASW for iron chloride (only 48% removal as compared to the >91 – 100% removals with the other two coagulants in

Figure 2.4A). The zeta potential of the TiO_2 was the greatest under these same conditions, suggesting highly stable particles. Specifically, the magnitude of zeta potential in ASW ranged from 42.4±2.5, 12.9±2.4, and 18±2.5 mV for $FeCl_3$, $FeSO_4$, and alum, respectively.

2.3.5 Size of TiO_2 Nanoparticles and Aggregates

Figure 6 presents the hydrodynamic diameter of the particles as measured by dynamic light scattering after each stage of treatment.

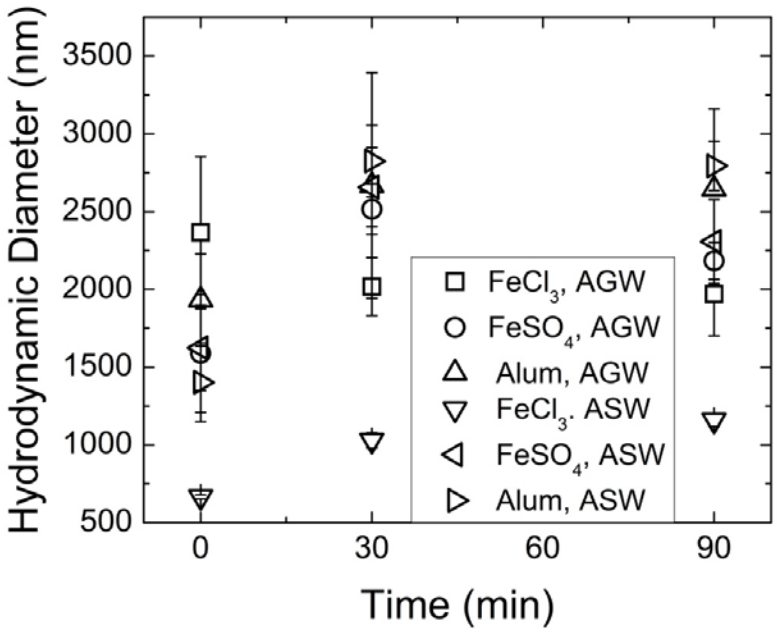

Figure 2.6. Hydrodynamic diameter values measured via dynamic light scattering (DLS) for particles remaining in suspension for artificial groundwater (AGW) and artificial surface water (ASW) after each stage of treatment (coagulation at 0 min, flocculation at 30 min, and sedimentation at 90 min). A concentration 100 mg/L TiO_2 and 50 mg/L dose of each coagulant was employed in all experiments.

As seen in Figure 2.6, TiO_2 aggregated to sizes on the order of ~2,000-2,700 nm for all cases except for $FeCl_3$ in ASW, which was ~1,200 nm. The hydrodynamic diameters measured correspond to the zeta potential data (Figure 2.5) in that under conditions where the particles exhibit greater zeta potential values, they are more stable and result in smaller measured diameters (lower DLS signal). Previous studies have also shown TiO_2 (100 mg/L) to aggregate anywhere from 1,000 nm to 3,000 nm in KCl during a similar time duration as this study (0 – 1.5 hours) (Chowdhury, Hong *et al.* 2011). Another group showed that aggregation occurs for zinc oxide (~ 400 nm), cerium dioxide (~1,000 nm), and titanium dioxide (~1,200 nm) nanoparticles in seawater and freshwater over a settling time of 60 minutes (Keller, Wang et al. 2010). Aggregation phenomena has also been observed in nanoscale zero-valent iron, which ranges anywhere between 125 nm to 1,200 nm with a nanoparticle concentration of 2 mg/L to 60 mg/L, respectively (Phenrat, Saleh et al. 2006). As observed from these examples, nanoparticle aggregation occurs regardless of solution chemistry and settling time.

2.4 Environmental Implications

This study provides evidence that typical primary treatment (coagulation, flocculation and sedimentation) can effectively remove metal oxide nanoparticles (i.e. TiO_2) within the range of concentrations tested in this work. Additionally, it was demonstrated that the total removal capacity at the scaled-down level resulted in the same removal capacity as the conventional scale system with $\geq$1-log removal for all three coagulants. Also, the ideal choice of coagulant is dependent on the water source. Based

on the results, $FeCl_3$ was more effective in total particle removal in AGW (> 95%) than in ASW (< 70%). Overall, $FeSO_4$ performed more effectively in ASW at all four TiO_2 concentrations tested (> 91%) than in AGW (>90 % at 50 and 100 mg/L; but 60-80% at 10 and 25 mg/L, respectively). Moreover, $Al_2(SO_4)_3$ was effective in both waters with similar removal results (nearly 100%). Based on the concentrations of metal coagulant used in this study, it is anticipated that removal via sweep flocculation is the dominant mechanism in particle removal (Duan and Gregory 2003; Gregory 2005). The effect of nanoparticle concentration was significant – generally, the higher TiO_2 concentrations (50 and 100 mg/L) were more effectively removed when compared to the lower concentrations (10 and 25 mg/L), and was also coagulant specific as discussed previously. This phenomenon suggests that a coagulant aid may be added to the low concentration systems to induce greater collision frequency between the nanoparticle and coagulant, as well as an appropriate scaling factor for the optimum dose of coagulant.

Mechanistically, electrokinetic interactions will also be important, as the relative charge on the particle surface in the various water conditions relate to particle stability. Electrostatic repulsion may occur due to the TiO_2 particles in water having a net positive surface charge at these solution conditions (Crittenden and Harza 2005). Bridging effects between the high amounts of divalent ions (Ca^{2+}, Mg^{2+}) and the metal coagulants may be occurring on the surface of TiO_2. Also, bridging affects the separation distance between the particles (Biggs 1995), and in turn, can cause larger aggregates of particles (Gregory 2005). Also, change in charge effects may be caused by the presence of ions due to the dissolved constituents in the two source waters. Complexation occurs in waters of high

ionic content and may induce the formation of ligands, which will solubilize metal complexes in water (Welton 1999; Crittenden and Harza 2005). Aluminum sulfate reacts with natural alkalinity in water to form aluminum hydroxo complexes (Viessman 2009) that also involve the production of H+ ions, which will lower the pH. These reactions are also analogous to the ferric-based coagulants with similar mechanisms (Viessman 2009). Furthermore, the source water impacts both the pH and ionic strength, and subsequently, affects the stability of the particles. The more acidic the solution is, the greater the zeta potential, and thus, a lower removal efficiency is observed. The decrease in pH observed in both source waters is due to chemical reactions associated with the metal coagulants. When salts of iron (Fe^{2+} or Fe^{3+}) or aluminum (Al^{3+}) ions are added to water, they will dissociate to yield trivalent Fe^{3+} or Al^{3+} and divalent Fe^{2+} (Crittenden and Harza 2005). These ions then hydrate to form aquometal or hydroxo complexes. During these reactions, the production of H^{+} will occur, which will depress the pH values (Viessman 2009).

Overall, results presented herein suggest that the chosen operating conditions and coagulant dose are critical based upon particle concentration levels and source waters. Environmentally relevant molecules such as natural organic matter may significantly impact operating parameters; therefore, further investigation is merited under such conditions. By understanding the optimum operating parameters and solution chemistries of these systems, best practices may be developed to remove TiO_2 (and other nanoparticles) via conventional water treatment methods before they enter the environment, and ultimately, drinking water supplies (Kumar 2012).

2.5 Acknowledgements

This work was supported by the National Science Foundation under Grant No. CBET-0954130. Any conclusions, findings, or opinions, recommendations, or suggestions expressed in this material are those of the authors and do not necessarily reflect the views of the National Science Foundation. We would also like to acknowledge Professor Mark Matsumoto and Dr. Nichola Kinsinger from the University of California, Riverside for providing guidance in the development of the project and manuscript, respectively.

2.6 Author Disclosure Statement

No competing financial interests exist.

2.7 References

Beltrán-Heredia, J., J. Sánchez-Martín, et al. (2009). "Anionic Surfactants Removal by Natural Coagulant/Flocculant Products." *Ind. Eng. Chem. Res.* **48**(10): 5085-5092.

Benjamin, M. M. (2002). Water Chemistry, McGraw-Hill Higher Education.

Biggs, S. (1995). "Steric and Bridging Forces between Surfaces Bearing Adsorbed Polymer: An Atomic Force Microscopy Study." Langmuir **11**(1): 156-162.

Bolster, C. H., A. L. Mills, et al. (1999). "Spatial distribution of deposited bacteria following Miscible Displacement Experiments in intact cores." *Water Resour. Res.* **35**(6): 1797-1807.

Bratby, J. (2006). Coagulation and Flocculation in Water and Wastewater Treatment, IWA Publishing.

Chen, D. and J. Li (2010). "Interfacial Functionalization of TiO2 with Smart Polymers: pH-Controlled Switching of Photocurrent Direction." *J. Phys. Chem. C* **114**(23): 10478-10483.

Chowdhury, I., Y. Hong, et al. (2011). "Mechanisms of TiO2 nanoparticle transport in porous media: Role of solution chemistry, nanoparticle concentration, and flowrate." *J. Colloid Interface Sci.* **360**(2): 548-555.

Crittenden, J. C. and M. W. Harza (2005). Water Treatment: Principles and Design, Wiley.

Dalai, S., S. Pakrashi, et al. (2012). "A comparative cytotoxicity study of TiO2 nanoparticles under light and dark conditions at low exposure concentrations." *Toxicol. Res.* **1**(2): 116-130.

Domingos, R. F., N. Tufenkji, et al. (2009). "Aggregation of Titanium Dioxide Nanoparticles: Role of a Fulvic Acid." *Environ. Sci. Technol.* **43**(5): 1282-1286.

Domínguez, J. R., J. Beltrán de Heredia, et al. (2005). "Evaluation of Ferric Chloride as a Coagulant for Cork Processing Wastewaters. Influence of the Operating Conditions on the Removal of Organic Matter and Settleability Parameters." *Ind. Eng. Chem. Fundam.* **44**(17): 6539-6548.

Duan, J. and J. Gregory (2003). "Coagulation by hydrolysing metal salts." *Adv. Colloid Interface Sci.* **100–102**(0): 475-502.

Duan, J., J. Wang, et al. (2002). "Coagulation of humic acid by aluminium sulphate in saline water conditions." Desalination **150**(1): 1-14.

Dunphy Guzman, K. A., M. P. Finnegan, et al. (2006). "Influence of Surface Potential on Aggregation and Transport of Titania Nanoparticles." *Environ. Sci. Technol.* **40**(24): 7688-7693.

French, R. A., A. R. Jacobson, et al. (2009). "Influence of Ionic Strength, pH, and Cation Valence on Aggregation Kinetics of Titanium Dioxide Nanoparticles." *Environ. Sci. Technol.* **43**(5): 1354-1359.

Gottschalk, F. and B. Nowack (2011). "The release of engineered nanomaterials to the environment." *J. Environ. Monit.* **13**(5): 1145-1155.

Gregory, J. (2005). Particles in Water: Properties and Processes, Taylor & Francis.

Keller, A., S. McFerran, et al. (2013). "Global life cycle releases of engineered nanomaterials." *J. Nanopart. Res.* **15**(6): 1-17.

Keller, A. A., H. Wang, et al. (2010). "Stability and Aggregation of Metal Oxide Nanoparticles in Natural Aqueous Matrices." *Environ. Sci. Technol.* **44**(6): 1962-1967.

Kim, E.-S., Y. Liu, et al. (2012). "Evaluation of Membrane Fouling for In-Line Filtration of Oil Sands Process-Affected Water: The Effects of Pretreatment Conditions." *Environ. Sci. Technol.* **46**(5): 2877-2884.

Kumar, A. (2012). "Making a Case for Human Health Risk-based Ranking Nanoparticles in Water for Monitoring Purposes." *Environ. Sci. Technol.* **46**(10): 5267-5268.

Lecoanet, H. F. and M. R. Wiesner (2004). "Velocity Effects on Fullerene and Oxide Nanoparticle Deposition in Porous Media." *Environ. Sci. Technol.* **38**(16): 4377-4382.

Lin, H., C. P. Huang, et al. (2006). "Size dependency of nanocrystalline TiO2 on its optical property and photocatalytic reactivity exemplified by 2-chlorophenol." *Appl. Catal., B* **68**(1–2): 1-11.

Linsebigler, A. L., G. Lu, et al. (1995). "Photocatalysis on TiO2 surfaces: principles, mechanisms, and selected results." *Chem. Rev.* **95**(3): 735-758.

Long, T. C., N. Saleh, et al. (2006). "Titanium Dioxide (P25) Produces Reactive Oxygen Species in Immortalized Brain Microglia (BV2): Implications for Nanoparticle Neurotoxicity†." *Environ. Sci. Technol.* **40**(14): 4346-4352.

Morfesis, A., A. M. Jacobson, et al. (2008). "Role of Zeta (ζ) Potential in the Optimization of Water Treatment Facility Operations." *Ind. Eng. Chem. Res.* **48**(5): 2305-2308.

Nel, A., T. Xia, et al. (2006). "Toxic Potential of Materials at the Nanolevel." Science **311**(5761): 622-627.

Palominos, R. A., A. Mora, et al. (2008). "Oxolinic acid photo-oxidation using immobilized TiO2." *J. Hazard. Mater.* **158**(2–3): 460-464.

Phenrat, T., N. Saleh, et al. (2006). "Aggregation and Sedimentation of Aqueous Nanoscale Zerovalent Iron Dispersions." *Environ. Sci. Technol.* **41**(1): 284-290.

Robichaud, C. O., A. E. Uyar, et al. (2009). "Estimates of Upper Bounds and Trends in Nano-TiO2 Production As a Basis for Exposure Assessment." *Environ. Sci. Technol.* **43**(12): 4227-4233.

Spellman, F. R. and J. Drinan (2000). The Drinking Water Handbook, Technomic Publishing Company.

Tchobanoglous, G., F. L. Burton, et al. (2003). Wastewater Engineering: Treatment and Reuse, McGraw-Hill Education.

Trouiller, B. R., R.; Westbrook, A.; Solaimani, P.; Schiestl, R.H. (2009). "Titanium dioxide nanoparticles induce DNA damage and genetic instability in vivo in mice." Cancer Res. **69**(22): 8784.

Viessman, W. (2009). Water Supply and Pollution Control, Prentice Hall Higher Education.

Weir, A., P. Westerhoff, et al. (2012). "Titanium Dioxide Nanoparticles in Food and Personal Care Products." *Environ. Sci. Technol.* **46**(4): 2242-2250.

Welton, T. (1999). "Room-Temperature Ionic Liquids. Solvents for Synthesis and Catalysis." *Chem. Rev.* **99**(8): 2071-2084.

Westerhoff, P., G. Song, et al. (2011). "Occurrence and removal of titanium at full scale wastewater treatment plants: implications for TiO2 nanomaterials." *J. Environ. Monit.* **13**(5): 1195-1203.

Wiesner, M. R., G. V. Lowry, et al. (2006). "Assessing the Risks of Manufactured Nanomaterials." *Environ. Sci. Technol.* **40**(14): 4336-4345.

Winter, T. C. (1999). Ground Water and Surface Water: A Single Resource, U.S. Geological Survey.

Xia, T., M. Kovochich, et al. (2008). "Comparison of the Mechanism of Toxicity of Zinc Oxide and Cerium Oxide Nanoparticles Based on Dissolution and Oxidative Stress Properties." ACS Nano **2**(10): 2121-2134.

Yang, H., M. Tong, et al. (2012). "Influence of Bentonite Particles on Representative Gram Negative and Gram Positive Bacterial Deposition in Porous Media." *Environ. Sci. Technol.* **46**(21): 11627-11634.

Yip, N. Y., A. Tiraferri, et al. (2011). "Thin-Film Composite Pressure Retarded Osmosis Membranes for Sustainable Power Generation from Salinity Gradients." *Environ. Sci. Technol.* **45**(10): 4360-4369.

Yu, W.-Z., J. Gregory, et al. (2010). "Breakage and Regrowth of Al-Humic Flocs - Effect of Additional Coagulant Dosage." *Environ. Sci. Technol.* **44**(16): 6371-6376.

Zhang, Y., Y. Chen, et al. (2008). "Stability of commercial metal oxide nanoparticles in water." *Water Res.* **42**(8-9): 2204-2212.

Zhao, H., H. Liu, et al. (2009). "Effect of Aluminum Speciation and Structure Characterization on Preferential Removal of Disinfection Byproduct Precursors by Aluminum Hydroxide Coagulation." *Environ. Sci. Technol.* **43**(13): 5067-5072.

Chapter 3

Titanium Dioxide (TiO_2) Nanoparticle Removal: Role of Coating, Natural Organic Matter, Source Water, and Solution Chemistry

Submitted to Environmental Engineering Science, Unpublished Work Copyright 2014

Honda, Ryan J., Keene, Valerie, Walker, Sharon L. "Titanium Dioxide (TiO_2) Nanoparticle Removal: Role of Coating, Natural Organic Matter, Source Water, and Solution Chemistry." *Environmental Engineering Science*. Submitted June 2014.

Abstract

As nanoparticles are considered emerging contaminants in water, there is a pressing need to ensure their removal. Specifically, recent studies have found titanium dioxide nanoparticles (TiO_2) to potentially cause adverse environmental and health effects. Traditional industrial treatment plants have three primary methods of treating and removing particles: coagulation, flocculation, and sedimentation. This study involves scaled-down jar tests with aluminum sulfate as a coagulant to determine the fundamental mechanisms involved in removal of bare and coated TiO_2 in a simple monovalent electrolyte (KCl), more complex waters (artificial groundwater and surface water, and in the presence of natural organic matter. Additional particle characterization measurements (zeta potential and hydrodynamic diameter) were performed to link stability to removal. Results showed that removal was most efficient in the presence of divalent cations ($Ca^{2+)}$ higher ionic strength, and in the absence of NOM and nanoparticle coating, achieving >1 log removal. However, as the system became more complex with the presence of nanoparticle coating and NOM, removal decreased to a maximum of ~80%. .

3.1 Introduction

Nanomaterials possess unique properties as compared to their larger (bulk) counterparts[1,2], transforming the design and manufacture of many consumer and industrial products. Due to these properties (electronic, optical, etc.), there are numerous commercial applications of nanomaterials such as cosmetics, drug delivery, electronics, sunscreens, and water purification technologies[3,4]. With increasing usage and hence the potential to enter natural and engineered environments through wastewater outfalls or industrial disposal processes, there is a growing concern regarding their fate and removal of them from groundwater and surface waters. Since engineered nanomaterials (ENMs) are considered a new class of environmental pollutants, current model paradigms and experimental approaches to determine the fate of them must be robust enough to ensure that they can appropriately predict ENM distribution in the environment[5].

An example of the most widely used ENMs is titanium dioxide (TiO_2), with an annual U.S. production rate of approximately 40,000 metric tons/year[6] and is steadily increasing every year[7]. One study found TiO_2 nanoparticles in wastewater effluent and biosolids with concentrations ranging anywhere from 0.01 mg/L – 3 mg/L[8]. Another study reported that concentrations ranged from about 0.2 – 1.2 mg/L in wastewater biosolids[9]. With TiO_2 is being detected in wastewater treatment effluent and biosolids, it may ultimately enter receiving bodies of water[9], which is of high interest to water treatment practitioners. According to a recent study by Keller *et al.* (2013), an in-depth analysis of the global life cycle release of engineered nanomaterials showed their distribution through various environments [10]. They estimated that 63–91% of about

300,000 metric tons of global ENM production in 2010 ended up in landfills, 8–28% in soils, 0.4–1.5% in water bodies, and 0.1– 1.5% into the atmosphere. Based on the various ENMs (TiO_2, ZnO, SiO_2, CeO_2, $Al2O_3$, Nano-Ag, Nano-Cu, Nano-Fe, and CNTs) that were investigated, it was reported that TiO_2 was by far the most significant ENM in terms of exposure based on estimated releases and use due to its many practical applications. The estimated global production of TiO_2 in 2010 consisted of about 39,600 metric tons/year in coatings, paints and pigments, and 30,800 metric tons/year in cosmetics alone. About 38,200, 15,600, 32,600, and 1,600 metric ton/year of TiO_2 were released into soil, water, landfill, and air, respectively. ZnO, one of the highest contributors of total ENM production for the same categories as TiO_2, had 5,780 metric tons/year in coatings, paints, and pigments, and 7,480 metric tons/year in cosmetics, respectively. About 8,700, 3,700, 21,100, and 600 metric tons per year were released into the same respective categories as TiO_2. Additionally, the Keller study showed that waste water treatment plants (WWTPs) were an important intermediate pathway from the ENMs to soil and water. Approximately 17-34% of ENMs were likely to pass through WWTPs, which lead to 3-25% of releases into water bodies via treated effluent and 44-47% of emissions to soils via biosolids. Based on the data, titania had the largest releases into soil, water, and air (followed by zinc and other metal oxides discussed in the study), particularly due to its low solubility. Hence, it is critical that the behavior and mechanisms of TiO_2 are identified in water treatment.

To understand TiO_2 fate and removal in water treatment, environmentally relevant conditions must be simulated with engineered particle coatings and the presence of

natural organic matter (NOM). A model NOM that has been utilized extensively in particle stability and transport studies is Suwannee River Humic Acid (SRHA). A negative surface potential is maintained around NOM in the natural environment since NOM consists of a complex mixture of polyelectrolytes that contain carboxylic and phenolic functional groups[11,12]. Due to these properties, NOM affects particle and aggregate sizes in suspension[12]. For example, previous studies have demonstrated NOM to contribute to electrostatic and electrosteric repulsion for TiO_2[13], increase stability of TiO_2[14,15] and gold nanoparticles[16], and decrease fullerene aggregation and deposition due to steric repulsion[17,18,19]. Based on these studies, it has been demonstrated that NOM plays a vital role in the behavior of nanomaterials by reducing the size of aggregates, contributing to steric and electrostatic effects, and increasing particle stability[20]. Other studies have also used SRHA as a representative NOM[14,16] in TiO_2 and gold nanoparticle stability tests. In addition to NOM, another factor that influences particle stability and aggregation is coating. For example, Chen *et al*. showed that alginate-coated (polysaccharides) hematite nanoparticles enhanced aggregation rates in the presence of divalent cations (Ca^{2+}, Sr^{2+}, and Ba^{2+}) due to attractive interactions (adhesion forces) between them and bridging effects that form larger alginate-hematite clusters[21,22]. In contrast, fullerene (C60) nanoparticle deposition rates (determined by Quartz-Crystal Microbalance) were significantly reduced in the presence of both humic acid and alginate coated silica surfaces due to steric repulsion as compared to in the absence of the polymers[18]. In industrial applications, nanoparticles are stabilized against aggregation through the adsorption of coatings[23]. A coating of particular interest is meso-2,3-

dimercaptosuccinic acid (DMSA), which has been used in a variety of biomedical and environmental applications. DMSA acts a chelating agent that is able to bind metal ions to form a complex ring structure called chelates, which possess ligand binding atoms that can form one or two covalent bonds[12]. DMSA forms strong complexes with the surface layer of the iron-oxide (maghemite) nanoparticles[24]. Previous work has shown DMSA to effectively act as a chelating agent for treatment of lead poisoning[25,26]. Other studies have demonstrated the use of DMSA as a capping agent for quantum dots[27] and iron-oxide nanoparticles[28,29]. It was also shown that DMSA-coated iron oxides had increased particle stability in intracellular uptake due to unbound carboxylate groups, which caused electrostatic repulsion between the charged nanoparticles. These studies show the importance of investigating nanoparticle fate in the presence of a coating; however, there are limited studies looking particle coating impacts on stability in an aquatic setting – particularly in the presence of NOM. Studies under these environmentally-relevant conditions with a model coating and humic acid are of vital importance to properly assess TiO_2 fate and removal that may be present in treated effluent.

The overall aim of this work was to identify the degree of removal of one of the most commonly used nanomaterials on the market (TiO_2) in aquatic conditions via scaled-down water treatment processes. Specifically, this work evaluates the removal of bare and DMSA-coated TiO_2 NP using one of the most commonly used coagulants[12] (alum) in both idealized aquatic conditions by employing previously optimized and scaled-down jar tests[30], which simulate the three primary stages (coagulation, flocculation, and sedimentation) of water treatment. ENM removal is quantified in the

presence or absence of natural organic matter (NOM) (i.e. Suwannee River Humic Acid). The objectives of this study were to (1) determine how key environmental parameters such as varying water chemistry (water type, ionic strength, etc.), particle coating, and the presence of NOM influence the removal TiO_2 NP, and (2) identify the various mechanisms involved in particle removal. By considering a broader number of relevant aquatic and nanoparticle parameters than investigated in the past, this study was designed to gain a greater understanding on nanomaterial removal mechanisms, with the goal that this may inform design and implementation of primary stages of water treatment.

3.2 Materials and Methods

3.2.1 TiO_2 Nanoparticles Preparation

Uncoated (bare) titanium dioxide (TiO_2) nanoparticles employed in this study were P25 Evonik Degussa (Evonik Industries AG, Germany). This TiO_2 is an industrial grade nanoparticle that has a phase composition of 82% rutile and 18% anatase with a purity of 99.5%. The average primary particle size, according to the manufacturer, was reported to be 21 nm. Prior to jar test experiments, a stock suspension of TiO_2 was prepared via a similar protocol by Chowdhury *et al.*, 2011[31]. The TiO_2 nanoparticles were sonicated (Transsonic 460/H, Barnstead Lab-Line, Melrose Park, IL) for ~2 min to help break-up aggregation immediately before jar test experiments. Coated TiO_2 nanoparticles were prepared by a similarly reported procedure[32] by utilizing meso-2,3-dimercaptosuccinic acid (DMSA) as the coating agent for P25 TiO_2.

3.2.2 Test Solutions

Four solution conditions were tested in this study: two ionic strengths (IS) of KCl, artificial groundwater, and artificial surface water. Monovalent electrolyte solutions (KCl) were used in this study at two different ionic strengths, 1.83 and 10 mM. These IS values were selected to compare to the ionic strengths of artificial surface water (ASW)[33] and groundwater (AGW)[34], respectively. The pH for all solutions was adjusted to 8±0.1 using 0.1 M KOH to mimic the pH of the AGW and ASW recipes used in this study. These simple monovalent electrolyte test solutions were created as a baseline comparison for the more complex source water recipes utilized. The complete list of constituents for AGW and ASW can be found in Table 3.1 below. All chemicals were either ACS grade reagents (purchased from Fisher Scientific, Fair Lawn, New Jersey) or research grade (from Mallinckrodt Chemical, Japan; and Acros Organics, New Jersey). For select experiments, a 1 mg/L of Suwannee River Humic Acid (SRHA) was used (International Humic Substances Society, MN). This concentration was selected since it represents a typical average of NOM present in groundwater and surface water[12].

Groundwater (IS = 10 mM)

Salt	mg/L
$CaCl_2\ 2H_2O$	107.1
$CaSO_4\ 2H_2O$	74.4
KNO_3	59.5
$NaHCO_3$	107.1
$Ca(NO_3)_2\ 4H_2O$	104.2
$MgSO_4\ 7H_2O$	178.6
Total:	630.9

Surface Water (IS = 1.83 mM)

Salt	mg/L
$MgCl_2\ 6H_2O$	16.5
$MgSO_4$	8.3
$KHCO_3$	3.0
$NaHCO_3$	19.3
$CaCO_3$	33.0
Total:	80.1

Table 3.1. Constituents for artificial groundwater[34] (AGW) and surface water[33] (ASW) recipes. Ionic strength (IS) of the final solutions is displayed at the top of the table.

3.2.3 Jar Test Experiments

Scaled-down jar tests[30] were used to simulate conventional coagulation, flocculation, and sedimentation processes. A single coagulant, aluminum sulfate (or alum, $Al_2(SO_4)_3$) at a dosage of 50 mg/L was used. To ensure that sufficient coagulant was present in the solution, the dissolved amount of metal species through speciation reactions was determined and is described in greater detail in the supporting information. The nanoparticle concentration (bare and coated) was 100 mg/L for all experiments. 1.5 mL samples were taken from the center point of the beaker at approximately 1 mm in depth in the beakers at the end of each stage of treatment for jar test experiments. Samples collected were used to evaluate particle concentration, zeta potential, and size. The samples taken at times 0, 30, and 90 min correspond to the end of the three stages of

treatment, where the absorbance was measured: 1 min for flash mixing, 30 min of flocculation, and 1 hr of sedimentation. Samples were measured in a UV-Vis spectrophotometer (DU Beckman Coulter, Fullerton, CA) at a wavelength of 370 nm. Other studies have successfully employed the use of a UV-Vis to measure the relative concentrations of nanoparticles[35,15].

3.2.4 Nanoparticle Characterization

Electokinetic characterization (zeta potential) and particle sizing (hydrodynamic diameter) was conducted using a ZetaPals Analyzer (Brookhaven Instruments Corp, Holtsville, NY). Zeta potential was determined from the Smoluchowski equation, which is applicable when the Debeye length (thickness of the double layer) of a particle is much less than the particle size[36,37]. Measurements were conducted immediately following the completion of each of the three treatment stages. Particle sizing was measured using Dynamic Light Scattering (DLS) (Brookhaven Model-BI-9000AT, Holtsville, NY). The zeta potential and hydrodynamic diameters were determined from the average of 5 runs, with each run lasting for two minutes. 2 mL of test samples were needed for characterization experiments. In total, 3.5 mL of samples are needed for measurements: 1.5 mL for absorption + 2 mL for characterization. Inductively Coupled Plasma Mass Spectroscopy (ICP-MS) (7700 Series, Agilent Technologies) measurements also were conducted to determine the concentration of TiO_2 remaining in suspension after the final sedimentation stage. Values are listed in Table 3.2.

Jar Tests and Conditions	ppm	Jar Tests and Conditions	ppm
AGW, 100 mg/L Bare TiO_2, Control	1.22086	AGW, 100 mg/L DMSA TiO_2, Control	1.10736
AGW, S1	1.09814	AGW, S1	1.10432
AGW, S2	1.09264	AGW, S2	1.10200
AGW, S3	1.09396	AGW, S3	1.09436
ASW, 100 mg/L Bare TiO_2, Control	1.10188	ASW, 100 mg/L DMSA TiO_2, Control	1.12905
ASW, S1	1.09985	ASW, S1	1.11770
ASW, S2	1.09284	ASW, S2	1.10995
ASW, S3	1.10096	ASW, S3	1.12104
1.83 mM KCl, 100 mg/L Bare TiO_2, Control	1.10204	1.83 mM KCl, 100 mg/L DMSA TiO_2, Control	1.11252
1.83 mM KCl, S1	1.09248	1.83 mM KCl, S1	1.10340
1.83 mM KCl, S2	1.09292	1.83 mM KCl, S2	1.10618
1.83 mM KCl, S3	1.09278	1.83 mM KCl, S3	1.10825
10mM KCl 100 mg/L Bare TiO_2 Control	1.11980	10mM KCl, 100 mg/L DMSA TiO_2, Control	1.11803
10 mM KCl, S1	1.10628	10 mM KCl, S1	1.10430
10 mM KCl, S2	1.10383	10 mM KCl, S2	1.10661
10 mM KCl S3	1.09240	10 mM KCl S3	1.10436
AGW, 100 mg/L Bare TiO_2 + NOM, Control	1.13041	AGW, 100 mg/L DMSA TiO_2 + NOM, Control	1.18561
AGW, S1	1.12414	AGW, S1	1.13007
AGW, S2	1.10947	AGW, S2	1.15308
AGW, S3	1.10727	AGW, S3	1.11327
ASW, 100 mg/L Bare TiO_2 + NOM, Control	1.12790	ASW, 100 mg/L DMSA TiO_2 + NOM, Control	1.27143
ASW, S1	1.10953	ASW, S1	1.14196
ASW, S2	1.10511	ASW, S2	1.16802
ASW, S3	1.10391	ASW, S3	1.11466
1.83 Mm KCl, 100 mg/L Bare TiO_2 + NOM, Control	1.12544	1.83 mM KCl, 100 mg/L DMSA TiO_2 + NOM, Control	1.12635
1.83 mM KCl, S1	1.11246	1.83 mM KCl, S1	1.12019
1.83 mM KCl, S2	1.10703	1.83 mM KCl, S2	1.11012
1.83 mM KCl, S3	1.10545	1.83 mM KCl, S3	1.11071
10 mM KCl, 100 mg/L Bare TiO_2 + NOM, Control	1.18861	10mM KCl, 100 mg/L DMSA TiO_2 + NOM, Control	1.15040
10 mM KCl, S1	1.15261	10 mM KCl, S1	1.11796
10 mM KCl, S2	1.14110	10 mM KCl, S2	1.10660
10 mM KCl S3	1.14448	10 mM KCl S3	1.10832
where,			
S1, S2, and S3 represent sedimentation in Jars 1, 2, and 3, respectively			
AGW = Artificial Groundwater			
ASW = Artificial Surface Water			
DMSA = meso-2,3-dimercaptosuccinic acid NP coating			
NOM = Natural Organic Matter at a constant concentration of 1 mg/L			

Table 3.2. ICP-MS data collected for jar tests after sedimentation. Experimental **c**onditions and parameters are listed in the table.

3.3 Results and Discussion

3.3.1 Effects of Ionic Strength and Solution Chemistry on Removal of Bare TiO_2 Nanoparticles

The first set of experiments consisted of using 1.83 and 10 mM KCl as the monovalent background solutions and 1.83 mM ASW and 10 mM AGW as the complex

water sources (Figure 3.1). Specifically, Figure 3.1 shows the total particle removal levels (A), zeta potentials (B), and hydrodynamic diameters (C), as a function of the four water sources at the different ionic strengths. Although total particle removal, zeta potential, and hydrodynamic diameter values were obtained (and are reported) after coagulation, flocculation, and sedimentation, the focal point for discussion will be at the end of sedimentation (90 min) as it is the final stage primary treatment.

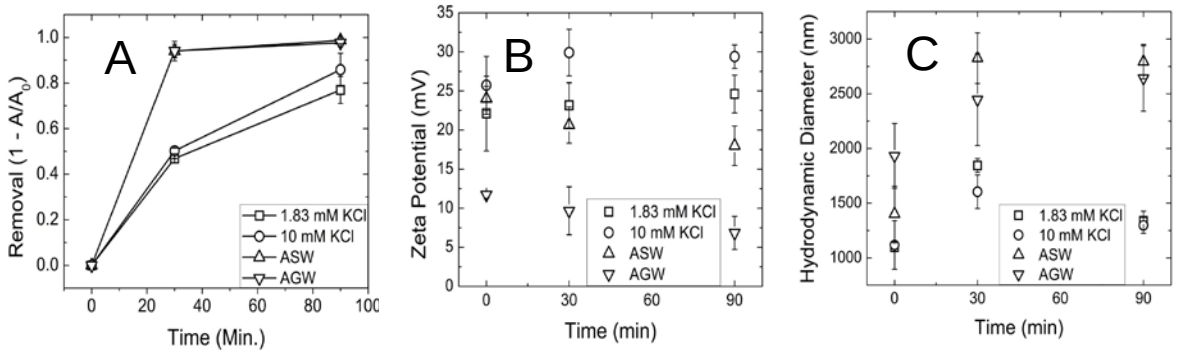

Figure 3.1. Bare TiO_2 removal was plotted in (A) against all four water sources: 1.83 mM KCl, 10 mM KCl, 1.83 mM ASW, and 10 mM AGW. The TiO_2 concentration was 100 mg/L. Coagulant (alum) dose remained constant at 50 mg/L. The operating parameters for the scaled-down jar tests were as follows: 1 min coagulation at 150 rpm, 30 min flocculation at 30 rpm, and 60 min sedimentation at 0 rpm. Zeta potential (mV) measurements were plotted (B) as a function of the four water sources at the end of each stage of treatment. Particle sizes (nm) were determined (C) in the four water sources at the end of each stage of treatment. Error bars indicate one standard deviation of three jar test measurements (A), five zeta potential measurements (B), and five DLS measurements (C).

Total bare particle removal in Figure 3.1A for 1.83 mM KCl, 10 mM KCl, AGW, and ASW was 77.0%±5.9%, 85.9%±7.2%, 97.6%±1.7%, and 98.7%±1.5%, respectively. As observed from this data, removal was more effective in the complex waters (AGW

and ASW) at both ionic strengths (IS) when compared to the simple monovalent electrolytes (1 and 10 mM KCl). Moreover, the removal at 10 mM KCl (85.9%±7.2%) was greater than at 1 mM KCl (77.0%±5.9%). At lower IS, the diffuse layer around the particle is extended and particles are prevented from coming into contact due to double-layer compression.[36] Conversely, at higher ionic salt concentrations, the diffuse layer becomes thinner and particles can approach more closely before any repulsion is felt. At closer approach, van der Waals attraction may be strong enough to outweigh double-layer repulsion.[36-37] These phenomenon likely explains why removal at higher IS was greater than the lower IS.

Relationships between removal trends and stability and size of the nanoparticles were observed by comparing their corresponding zeta potentials and hydrodynamic diameters. Zeta potential in Figure 3.1B for 1.83 mM KCl, 10 mM KCl, AGW, and ASW was 24.6±2.4 mV, 29.4±1.5 mV, 6.8±2.1 mV, and 18.0±2.5 mV, respectively. Particle size in Figure 3.1C for 1.83 mM KCl, 10 mM KCl, AGW, and ASW was 1341.0±95.9 nm, 1297.0±71.9 nm, 2644.6±515.2 nm, and 2793.8±158.0 nm, respectively. Similar TiO_2 stability trends where ionic strength is low have been reported in literature with TiO_2 in KCl[31] and in more complex waters[15]. Other studies have also reported enhanced metal oxide nanoparticle stability at low ionic strengths[38, 39, 40,41]. The greater magnitude of zeta potentials observed in KCl indicated higher particle stability and poorer removals. Additionally, particle sizes were smaller in the KCl suspensions compared to AGW and ASW, which also corresponded to poorer removal (i.e. smaller particles did not settle as well the larger particles). In addition to ionic strength effects,

the presence of divalent cations (i.e. Ca^{2+}) in solution affects particle stability[42], and thus, will impact removal efficiency in the case of AGW and ASW in this study. Ca^{2+} ions lead to greater electrical double layer compression than monovalent ions because of its large outer valence shell size, and can induce greater bridging effects between particles[36]. As such, the presence of Ca^{2+} in suspensions leads to greater aggregation and electrostatic attraction towards the surface. This phenomenon is most likely due to charge screening and reduced Debye length[36,37]. As observed in Figure 3.1, removal was greatest (>98%) in AGW and ASW where calcium was the most predominate divalent cation species present in those source waters. Additionally, the particle sizes were notably larger (>2,500 nm) in AGW and ASW when compared to the monovalent KCl solutions. Previous studies have also demonstrated similar effects where calcium ions contributed to enhanced nanoparticle aggregation and larger particle sizes[21,22, 38,43,44].

3.3.2 Role of Natural Organic Matter (NOM) on Removal of Bare TiO_2 Nanoparticles

To simulate a more environmentally relevant scenario, the role of natural organic matter (SRHA) on the removal of bare TiO_2 as a function of the four water sources (1.83 mM KCl, 10 mM KCl, AGW, and ASW) was investigated. The data is shown in Figure 3.2A. Total particle removal in the presence of NOM in Figure 3.2A for 1.83 mM KCl, 10 mM KCl, AGW, and ASW was 90.8%±0.9%, 23.0%±9.3%, 74.9%±1.1%, and 80.4%±2.6%, respectively. Removal in AGW and ASW was approximately 75-80%, whereas >90% in 1.83 mM KCl. However, removal was notably lowest in the 10 mM

KCl suspension. This phenomenon may be attributed due the anticipated compression of the electric double layer occurring with an increase of ionic strength (10 mM vs. 1.83 mM).

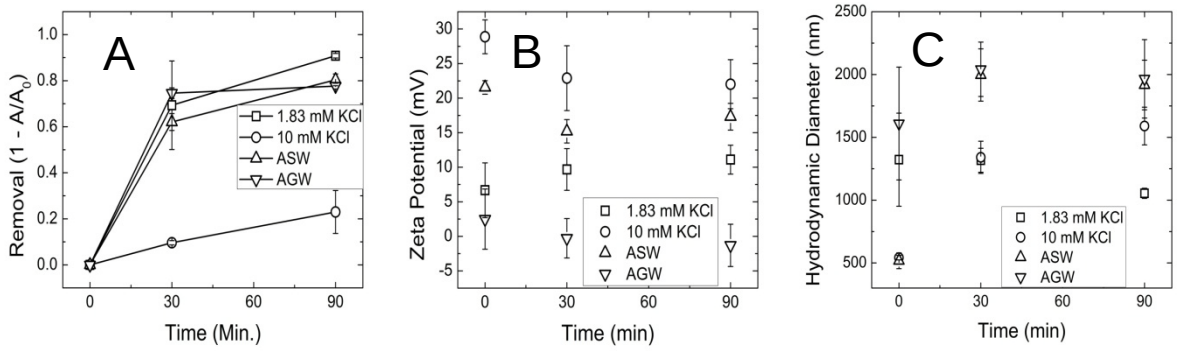

Figure 3.2. Bare TiO_2 + SRHA removal was plotted in (A) against all four water sources: 1.83 mM KCl, 10 mM KCl, 1.83 mM ASW, and 10 mM AGW. The TiO_2 concentration was 100 mg/L. Coagulant (alum) dose remained constant at 50 mg/L. The operating parameters for the scaled-down jar tests were as follows: 1 min coagulation at 150 rpm, 30 min flocculation at 30 rpm, and 60 min sedimentation at 0 rpm. Zeta potential (mV) measurements were plotted (B) as a function of the four water sources at the end of each stage of treatment. Particle sizes (nm) were determined (C) in the four water sources at the end of each stage of treatment. Error bars indicate one standard deviation of three jar test measurements (A), five zeta potential measurements (B), and five DLS measurements (C).

Zeta potential in Figure 3.2B for 1.83 mM KCl, 10 mM KCl, AGW, and ASW was 11.1±2.1 mV, 22.0±3.5 mV, -1.3±3.1 mV, and 17.3±1.9 mV, respectively. The greatest zeta potential occurred in the 10 mM KCl solution, which correlates to the poor removal in Figure 3.2A due to enhanced particle stability. Particle size in Figure 3.2C for 1.83 mM KCl, 10 mM KCl, AGW, and ASW was 1054.5±40.5 nm, 1590.2±150.2 nm,

1966.1±312.1 nm, and 1916.8±197.8 nm, respectively. Particle sizes became larger as a function of increasing water complexity.

Similar stability data has been previously reported in literature. For example, due to the combined effect of electrostatic and steric repulsion forces, the presence of SRHA increased the stability (zeta potentials between -5 to -45 mV) of TiO_2 in NaCl and $CaCl_2$ over a range of ionic strengths and pH[13] in a QCM-D. Another study reported that the deposition kinetics of fullerene (C60) nanoparticles were significantly slowed in presence of humic acids due to steric repulsion[18]. Additionally, they observed that in the presence of $CaCl_2$, the deposition kinetics of the C60 nanoparticles onto humic acid-coated surfaces to be high due to macromolecules undergoing complex formation with calcium ions, reducing the charge and steric influences of the adsorbed macromolecular layers. It has also been reported that the presence of SRHA had a greater stabilizing influence on TiO_2 than bacteria, and that nanoparticle transport resulted in much less deposition, indicating a complex combination of interactions involving particle stabilization[14]. Furthermore, they demonstrated the presence of Ca^{2+} to play a significant role in these interactions and promoted formation of large clusters of TiO_2, NOM, and bacteria. Since NOM consists of a complex mixture of polyelectrolyes and carboxylic/phenolic functional groups, it typically maintains a negative surface potential in natural water environments[12]. Another group investigated how NOM increased TiO_2 nano-composite stability and that also increased salt concentrations were needed to destabilize the suspension during flocculation[45]. Association with NOM, along with ion valence, has been known to influence particle stability due to these properties described. These

factors described, further validates the mechanisms and phenomena occurring during the removal experiments in this study, reaffirming the significant role NOM plays in nanoparticle stability.

3.3.3 Role of DMSA Coating and NOM on Removal of TiO_2 Nanoparticles

The most environmentally complex yet relevant conditions of this study include the presence of both particle coating and natural organic matter. The results discussed up until now have looked at the removal of bare (uncoated) TiO_2. Another interesting aspect of this study was to determine how DMSA-coated TiO_2 would behave in similar conditions to what was previously described. Total removal of DMSA-coated particles are shown in Figure 3.3A for 1.83 mM KCl, 10 mM KCl, AGW, and ASW, and was 85.0%±2.8%, 85.8%±12.0%, 98.5%±0.6%, and 74.9%±1.6%, respectively. Zeta potential in Figure 3.3B for 1.83 mM KCl, 10 mM KCl, AGW, and ASW was 24.7±2.5 mV, 25.7±4.2 mV, 8.0±2.1 mV, and 19.1±2.6 mV, respectively. The magnitude of zeta potential was similar in all cases, except in AGW; the smaller zeta potential corresponded to greater removal. Particle size in Figure 3.3C for 1.83 mM KCl, 10 mM KCl, AGW, and ASW was 897.0±38.6 nm, 1192.1±101.7 nm, 2800.2±970.4 nm, and 1615.0±156.4 nm, respectively. Lastly, particle sizes remained constant in all water sources except for AGW, in which the sizes were notably larger, leading to enhanced removal.

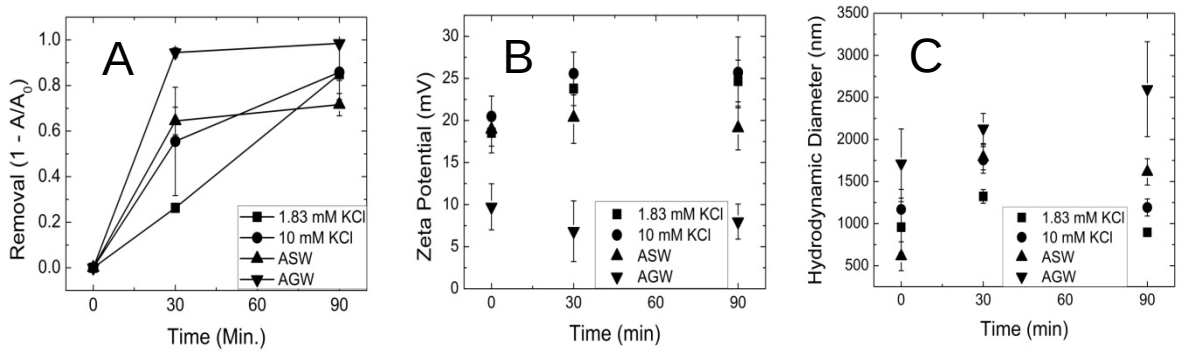

Figure 3.3. DMSA-coated TiO_2 removal was plotted in (A) against all four water sources: 1.83 mM KCl, 10 mM KCl, 1.83 mM ASW, and 10 mM AGW. The TiO_2 concentration was 100 mg/L. Coagulant (alum) dose remained constant at 50 mg/L. The operating parameters for the scaled-down jar tests were as follows: 1 min coagulation at 150 rpm, 30 min flocculation at 30 rpm, and 60 min sedimentation at 0 rpm. Zeta potential (mV) measurements were plotted (B) as a function of the four water sources at the end of each stage of treatment. Particle sizes (nm) were determined (C) in the four water sources at the end of each stage of treatment. Error bars indicate one standard deviation of three jar test measurements (A), five zeta potential measurements (B), and five DLS measurements (C).

Total coated particle and NOM removal in Figure 3.4A for 1.83 mM KCl, 10 mM KCl, AGW, and ASW was 89.1%±5.0%, 84.9%±4.0%, 71.8%±3.0%, and 68.7%±3.4%, respectively. Removal decreased as a function of increasing water source complexity. Zeta potential in Figure 3.4B for 1.83 mM KCl, 10 mM KCl, AGW, and ASW was 8.2±3.2 mV, 5.6±6.0 mV, -3.1±5.6 mV, and 16.5±2.5 mV, respectively. The greatest zeta potential in ASW corresponded to the poorest removal as indicated by greater particle stability when compared to the other three water sources. Typically, the presence of nanoparticle coating and natural organic matter stabilize particles in suspension. Particle size in Figure 3.4C for 1.83 mM KCl, 10 mM KCl, AGW, and ASW was

1256.7±80.7 nm, 1288.6±60.2 nm, 1712.1±173.4 nm, and 2741.7 nm, respectively. Particle sizes became larger as a function of water complexity.

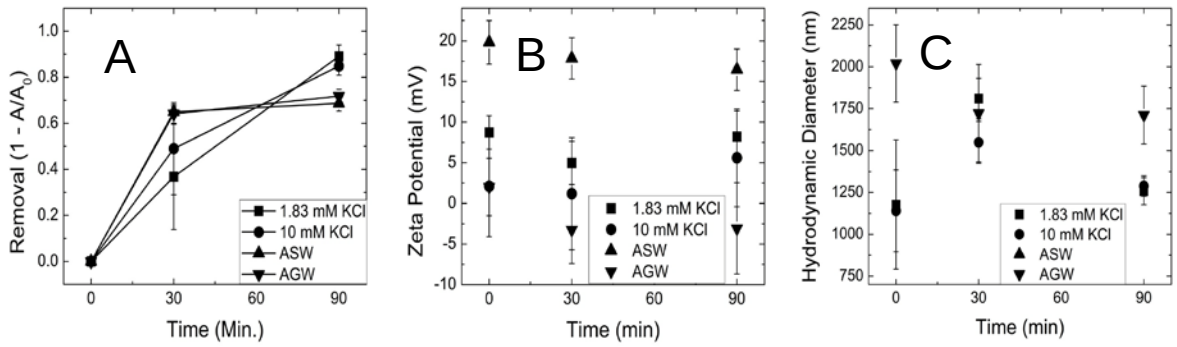

Figure 3.4. DMSA-coated TiO_2 + SRHA removal was plotted in (A) against all four water sources: 1.83 mM KCl, 10 mM KCl, 1.83 mM ASW, and 10 mM AGW. The TiO_2 concentration was 100 mg/L. Coagulant (alum) dose remained constant at 50 mg/L. The operating parameters for the scaled-down jar tests were as follows: 1 min coagulation at 150 rpm, 30 min flocculation at 30 rpm, and 60 min sedimentation at 0 rpm. Zeta potential (mV) measurements were plotted (B) as a function of the four water sources at the end of each stage of treatment. Particle sizes (nm) were determined (C) in the four water sources at the end of each stage of treatment. Error bars indicate one standard deviation of three jar test measurements (A), five zeta potential measurements (B), and five DLS measurements (C).

As observed and discussed in sections 3.3.1 and 3.3.2 previously, removal was generally most efficient in the systems with calcium ions (AGW and ASW) without the presence of humic acid or particle coating. As seen in this section, the combination of NOM and particle coating contributed greatest particle stability (lowest particle sizes and smallest magnitude of zeta potential), and hence, the poorest removal compared to Figures 3.1 and 3.2. The greatest removal was only ~80% in both ionic strengths of KCl and ~70% in AGW and ASW. One-log removal was not achieved in the presence of DMSA-coated TiO_2 + NOM under any condition. This phenomenon suggests that a

combination of complex mechanisms and stabilization affected removal. Steric interactions due to NOM may cause the TiO_2 nanoparticles to repel one another due to the increased amount of negative surface charges present. Bridging effects between the coagulant aluminum ions, NOM, and coating may be causing decreased site competition, leading to increased nanoparticle stabilization[12,36]. Also, charge reversal effects may influence particle removal since there are many different charges (due to the many charged constituents in water sources, precipitation of aluminum, NOM) in the suspensions.

3.4 Environmental Implications

In this study, it was determined that ionic strength, solution chemistry, and water type significantly impacted the removal and stability of TiO_2. Additionally, the impact of environmentally relevant factors such as the presence of humic acids and particle coating hindered total particle removal. Bare TiO_2 was removed the most effectively, while DMSA-particle coating and SRHA enhanced particle stability. From the colloidal literature, it is known that increasing the salt concentration in solution screens the repulsive electrostatic interactions between particles through compression of the electrical double layer that surrounds a charged particle[36,37]. Moreover, the critical salt concentration above which attractive forces become predominant (critical coagulation concentration), determines the degree of colloidal stability[11]. Salt addition helps induce neighboring particles to come closer to one another, which could be a prerequisite condition or mechanism for NOM-induced bridging flocculation. This study observed

how coating and NOM influenced stability of the particles. The more stable (smaller magnitude of zeta potential), the greater the aggregate size. The overall aggregate size maybe similar, but the differing primary particle size changes the reactivity of that aggregate and its sensitivity to the chemical nature of the system [46]. From this study, it is of critical importance to understand how governing chemical and physical mechanisms (polymer bridging, electrostatic forces, charge neutralization, orthokinetic/perikinetic forces, sweep flocculation) affect removal capacity of nanomaterials based on the various conditions (i.e. ionic strength, solution chemistry, pH, water type). As such, our study has systematically considered these many but significant factors when investigating TiO_2 removal. Understanding these mechanisms will lead to enhanced effectiveness and optimization of experimental parameters during the particle removal process in groundwater or subsurface environments.

3.5 Acknowledgements

This study was supported by the National Science Foundation under Grant No. CBET-0954130. Any conclusions, findings, recommendations, or suggestions expressed in this research are those of the authors and may not reflect the views of the National Science Foundation. We would like to acknowledge Dr. Mark Matsumoto from the University of California, Riverside for providing helpful insight into operating conditions and relevant parameters in the jar tests. Additionally, we would like to thank Dr. Haizhou Liu and his graduate student, Lucy Liu, for their help with conducting ICP-MS experiments.

3.6 Author Disclosure Statement

No competing financial interests exist.

3.7 References

1. Alivisatos, A. P., Semiconductor Clusters, Nanocrystals, and Quantum Dots. *Science* **1996,** *271* (5251), 933-937.

2. Nel, A.; Xia, T.; Mädler, L.; Li, N., Toxic Potential of Materials at the Nanolevel. *Science* **2006,** *311* (5761), 622-627.

3. Dunphy Guzmán, K. A.; Taylor, M. R.; Banfield, J. F., Environmental Risks of Nanotechnology: National Nanotechnology Initiative Funding, 2000−2004. *Environmental Science & Technology* **2006,** *40* (5), 1401-1407.

4. Wiesner, M. R.; Lowry, G. V.; Alvarez, P.; Dionysiou, D.; Biswas, P., Assessing the Risks of Manufactured Nanomaterials. *Environ. Sci. Technol.* **2006,** *40* (14), 4336-4345.

5. Westerhoff, P.; Nowack, B., Searching for Global Descriptors of Engineered Nanomaterial Fate and Transport in the Environment. *Acc. Chem. Res.* **2012,** *46* (3), 844-853.

6. Savage, N.; Thomas, T. A.; Duncan, J. S., Nanotechnology applications and implications research supported by the US Environmental Protection Agency STAR grants program. *Journal of Environmental Monitoring* **2007,** *9* (10), 1046-1054.

7. Weir, A.; Westerhoff, P.; Fabricius, L.; Hristovski, K.; von Goetz, N., Titanium Dioxide Nanoparticles in Food and Personal Care Products. *Environ. Sci. Technol.* **2012,** *46* (4), 2242-2250.

8. Kiser, M. A.; Westerhoff, P.; Benn, T.; Wang, Y.; Pérez-Rivera, J.; Hristovski, K., Titanium Nanomaterial Removal and Release from Wastewater Treatment Plants. *Environmental Science & Technology* **2009,** *43* (17), 6757-6763.

9. Westerhoff, P.; Song, G.; Hristovski, K.; Kiser, M. A., Occurrence and removal of titanium at full scale wastewater treatment plants: implications for TiO2 nanomaterials. *J. Environ. Monit.* **2011,** *13* (5), 1195-203.

10. Keller, A.; McFerran, S.; Lazareva, A.; Suh, S., Global life cycle releases of engineered nanomaterials. *J. Nanopart. Res.* **2013,** *15* (6), 1-17.

11. Viessman, W., *Water Supply and Pollution Control*. Prentice Hall Higher Education: 2009.

12. Crittenden, J. C.; Harza, M. W., *Water Treatment: Principles and Design*. Wiley: 2005.

13. Thio, B. J. R.; Zhou, D.; Keller, A. A., Influence of natural organic matter on the aggregation and deposition of titanium dioxide nanoparticles. *Journal of Hazardous Materials* **2011,** *189* (1–2), 556-563.

14. Chowdhury, I.; Cwiertny, D. M.; Walker, S. L., Combined Factors Influencing the Aggregation and Deposition of nano-TiO2 in the Presence of Humic Acid and Bacteria. *Environ. Sci. Technol.* **2012,** *46* (13), 6968-6976.

15. Keller, A. A.; Wang, H.; Zhou, D.; Lenihan, H. S.; Cherr, G.; Cardinale, B. J.; Miller, R.; Ji, Z., Stability and Aggregation of Metal Oxide Nanoparticles in Natural Aqueous Matrices. *Environ. Sci. Technol.* **2010,** *44* (6), 1962-1967.

16. Stankus, D. P.; Lohse, S. E.; Hutchison, J. E.; Nason, J. A., Interactions between Natural Organic Matter and Gold Nanoparticles Stabilized with Different Organic Capping Agents. *Environ. Sci. Technol.* **2010,** *45* (8), 3238-3244.

17. Chen, Z.; Westerhoff, P.; Herckes, P., Quantification of C60 fullerene concentrations in water. *Environ. Toxicol. Chem.* **2008,** *27* (9), 1852-1859.

18. Chen, K. L.; Elimelech, M., Interaction of Fullerene (C60) Nanoparticles with Humic Acid and Alginate Coated Silica Surfaces: Measurements, Mechanisms, and Environmental Implications. *Environmental Science & Technology* **2008,** *42* (20), 7607-7614.

19. Chen, K. L.; Elimelech, M., Aggregation and Deposition Kinetics of Fullerene (C60) Nanoparticles. *Langmuir* **2006,** *22* (26), 10994-11001.

20. Petosa, A. R.; Jaisi, D. P.; Quevedo, I. R.; Elimelech, M.; Tufenkji, N., Aggregation and Deposition of Engineered Nanomaterials in Aquatic Environments: Role of Physicochemical Interactions. *Environ. Sci. Technol.* **2010,** *44* (17), 6532-6549.

21. Chen, K. L.; Mylon, S. E.; Elimelech, M., Enhanced Aggregation of Alginate-Coated Iron Oxide (Hematite) Nanoparticles in the Presence of Calcium, Strontium, and Barium Cations. *Langmuir* **2007,** *23* (11), 5920-5928.

22. Chen, K. L.; Mylon, S. E.; Elimelech, M., Aggregation Kinetics of Alginate-Coated Hematite Nanoparticles in Monovalent and Divalent Electrolytes. *Environmental Science & Technology* **2006,** *40* (5), 1516-1523.

23. Joo, S. H.; Al-Abed, S. R.; Luxton, T., Influence of Carboxymethyl Cellulose for the Transport of Titanium Dioxide Nanoparticles in Clean Silica and Mineral-Coated Sands. *Environmental Science & Technology* **2009,** *43* (13), 4954-4959.

24. Wilhelm, C.; Billotey, C.; Roger, J.; Pons, J. N.; Bacri, J. C.; Gazeau, F., Intracellular uptake of anionic superparamagnetic nanoparticles as a function of their surface coating. *Biomaterials* **2003,** *24* (6), 1001-1011.

25. Aposhian Hv Fau - Aposhian, M. M.; Aposhian, M. M., meso-2,3-Dimercaptosuccinic acid: chemical, pharmacological and toxicological properties of an orally effective metal chelating agent. (0362-1642 (Print)).

26. Asiedu, P.; Moulton T Fau - Blum, C. B.; Blum Cb Fau - Roldan, E.; Roldan E Fau - Lolacono, N. J.; Lolacono Nj Fau - Graziano, J. H.; Graziano, J. H., Metabolism of meso-2,3-dimercaptosuccinic acid in lead-poisoned children and normal adults. (0091-6765 (Print)).

27. Sevinc, E.; Ertas, F. S.; Ulusoy, G.; Ozen, C.; Acar, H. Y., Meso-2,3-dimercaptosuccinic acid: from heavy metal chelation to CdS quantum dots. *J. Mater. Chem.* **2012,** *22* (11), 5137-5144.

28. Chen, Z. P.; Zhang, Y.; Zhang, S.; Xia, J. G.; Liu, J. W.; Xu, K.; Gu, N., Preparation and characterization of water-soluble monodisperse magnetic iron oxide nanoparticles via surface double-exchange with DMSA. *Colloids Surf., A* **2008,** *316* (1–3), 210-216.

29. Kima, M.; Lima, B.; Jeongb, Y.; Choa, Y.; Choaa, Y., Surface modification of magnetite nanoparticles for immobilization with lysozyme. *J. Ceram. Process. Res.* **2007,** *8* (4), 293-295.

30. Honda, R. J.; Keene, V.; Daniels, L.; Walker, S. L., Removal of TiO2 Nanoparticles During Primary Water Treatment: Role of Coagulant Type, Dose, and Nanoparticle Concentration. *Environ. Eng. Sci.* **2014,** *31* (3), 127-134.

31. Chowdhury, I.; Hong, Y.; Honda, R. J.; Walker, S. L., Mechanisms of TiO2 nanoparticle transport in porous media: Role of solution chemistry, nanoparticle concentration, and flowrate. *J. Colloid Interface Sci.* **2011,** *360* (2), 548-555.

32. Maurizi, L.; Bisht, H.; Bouyer, F.; Millot, N., Easy Route to Functionalize Iron Oxide Nanoparticles via Long-Term Stable Thiol Groups. *Langmuir* **2009,** *25* (16), 8857-8859.

33. Yip, N. Y.; Tiraferri, A.; Phillip, W. A.; Schiffman, J. D.; Hoover, L. A.; Kim, Y. C.; Elimelech, M., Thin-Film Composite Pressure Retarded Osmosis Membranes for Sustainable Power Generation from Salinity Gradients. *Environ. Sci. Technol.* **2011,** *45* (10), 4360-4369.

34. Bolster, C. H.; Mills, A. L.; Hornberger, G. M.; Herman, J. S., Spatial distribution of deposited bacteria following Miscible Displacement Experiments in intact cores. *Water Resour. Res.* **1999,** *35* (6), 1797-1807.

35. Dalai, S.; Pakrashi, S.; Kumar, R. S. S.; Chandrasekaran, N.; Mukherjee, A., A comparative cytotoxicity study of TiO2 nanoparticles under light and dark conditions at low exposure concentrations. *Toxicol. Res.* **2012,** *1* (2), 116-130.

36. Gregory, J., *Particles in Water: Properties and Processes*. Taylor & Francis: 2005.

37. Elimelech, M.; Jia, X.; Gregory, J.; Williams, R., *Particle Deposition & Aggregation: Measurement, Modelling and Simulation*. Elsevier Science: 1998.

38. French, R. A.; Jacobson, A. R.; Kim, B.; Isley, S. L.; Penn, R. L.; Baveye, P. C., Influence of Ionic Strength, pH, and Cation Valence on Aggregation Kinetics of Titanium Dioxide Nanoparticles. *Environ. Sci. Technol.* **2009,** *43* (5), 1354-1359.

39. Fang, J.; Shan, X. Q.; Wen, B.; Lin, J. M.; Owens, G., Stability of titania nanoparticles in soil suspensions and transport in saturated homogeneous soil columns. *Environ. Pollut.* **2009,** *157* (4), 1101-9.

40. Chowdhury, I.; Walker, S. L.; Mylon, S. E., Aggregate morphology of nano-TiO2: role of primary particle size, solution chemistry, and organic matter. *Environ. Sci.: Processes & Impacts* **2013,** *15* (1), 275-282.

41. Lanphere, J. D.; Luth, C. J.; Walker, S. L., Effects of Solution Chemistry on the Transport of Graphene Oxide in Saturated Porous Media. *Environmental Science & Technology* **2013,** *47* (9), 4255-4261.

42. Benjamin, M. M., *Water Chemistry*. McGraw-Hill Higher Education: 2002.

43. Quevedo, I. R.; Tufenkji, N., Mobility of Functionalized Quantum Dots and a Model Polystyrene Nanoparticle in Saturated Quartz Sand and Loamy Sand. *Environmental Science & Technology* **2012,** *46* (8), 4449-4457.

44. Torkzaban, S.; Bradford, S. A.; Wan, J.; Tokunaga, T.; Masoudih, A., Release of Quantum Dot Nanoparticles in Porous Media: Role of Cation Exchange and Aging Time. *Environmental Science & Technology* **2013,** *47* (20), 11528-11536.

45. Labille, J.; Feng, J.; Botta, C.; Borschneck, D.; Sammut, M.; Cabie, M.; Auffan, M.; Rose, J.; Bottero, J.-Y., Aging of TiO2 nanocomposites used in sunscreen. Dispersion and fate of the degradation products in aqueous environment. *Environ. Pollut.* **2010,** *158* (12), 3482-3489.

46. Jassby, D.; Farner Budarz, J.; Wiesner, M., Impact of Aggregate Size and Structure on the Photocatalytic Properties of TiO2 and ZnO Nanoparticles. *Environ. Sci. Technol.* **2012,** *46* (13), 6934-6941.

Chapter 4

Development of a Micromodel Flow Cell for 2D Pore-scale Visualization of Filtration Processes

Ryan Honda and Sharon L. Walker

4.1 Introduction

With high levels of production and application of nanomaterials in such products as cosmetics, textiles, electronics, detergents, and textiles, there are growing concerns of them being released in the environment[1,2,3,4]. Fate and transport studies have been conducted extensively with the use of saturated and unsaturated columns that simulate soil environments. Specifically, column studies have investigated nanomaterial transport and filtration processes of TiO_2[5,6], graphene oxide[7], iron-oxide[6, 8], single-walled carbon nanotubes[9], fullerenes[10], and quantum dots[11] using macro-sized packed-bed columns. While column experiments provide useful information – such as nanoparticle breakthrough (elution), retention, and solution chemistry behavior (i.e. effects of pH, ionic strength, electrolyte) – understanding of the mechanistic phenomena such as attachment, deposition, straining, blocking, and other intermolecular forces at the pore-scale level is limited. Therefore, to understand such mechanisms, the use of a 2D micromodel flow cell is needed.

A micromodel flow cell allows for 2D pore-scale visualization of colloids (i.e. nanoparticles, bacteria) through porous media that simulates collector sand grains of a packed-bed column. Previous work has been employed to develop and fabricate such micromodels[12,13,14,15]. Studies have utilized silicon fabricated micromodels to observe transport and attachment of *Cryptosporidium parvuum* oocysts[16,17], *Azotobacter vinelandii*[18], and polystyrene latex particles (>3 μm)[13]. In all of these studies mentioned, real-time images were taken over a certain experimental duration of time and evaluated

for the mass transfer of particles to the collector surfaces. By being able to count the number of particles attached, the single collector efficiency and attachment efficiency were calculated. These values allow for a quantitative evaluation of the mechanistic behavior at the pore-scale level, which cannot be directly observed in a macro-scale (3D) column experiment. However, to date, this method has not been employed for nano-sized particles. *To our knowledge, there are no studies that involve pore-scale visualization of nanoparticles using micromodels, and no work correlating the 2D to 3D systems.*

The overall aim of this project was to design, fabricate, and demonstrate a 2D micromodel flow cell as a means to investigate nanoparticle filtration. Specifically, this method was selected to allow direct visualization of pore-scale physico-chemical processes by using an array of 2D silica cylinders through which a model nanoparticle (i.e. 20 nm fluorescent latex microspheres or fluorescently labeled engineered nanoparticles) can be transported. Through the creation of this system, future studies can directly compare filtration phenomena to a 3D macro-scale column experiment. The objectives of this research were 1) develop and fabricate silica micromodels in a cleanroom facility, 2) construct a manifold assembly to properly house the micromodel, 3) create a cleaning protocol, 4) demonstrate the technique by calculating single collector efficiency and attachment efficiency for a model nanoparticle, and 5) compare attachment between our micromodel and published data from column experiments. The entire micromodel schematic is seen below in Figure 4.1.

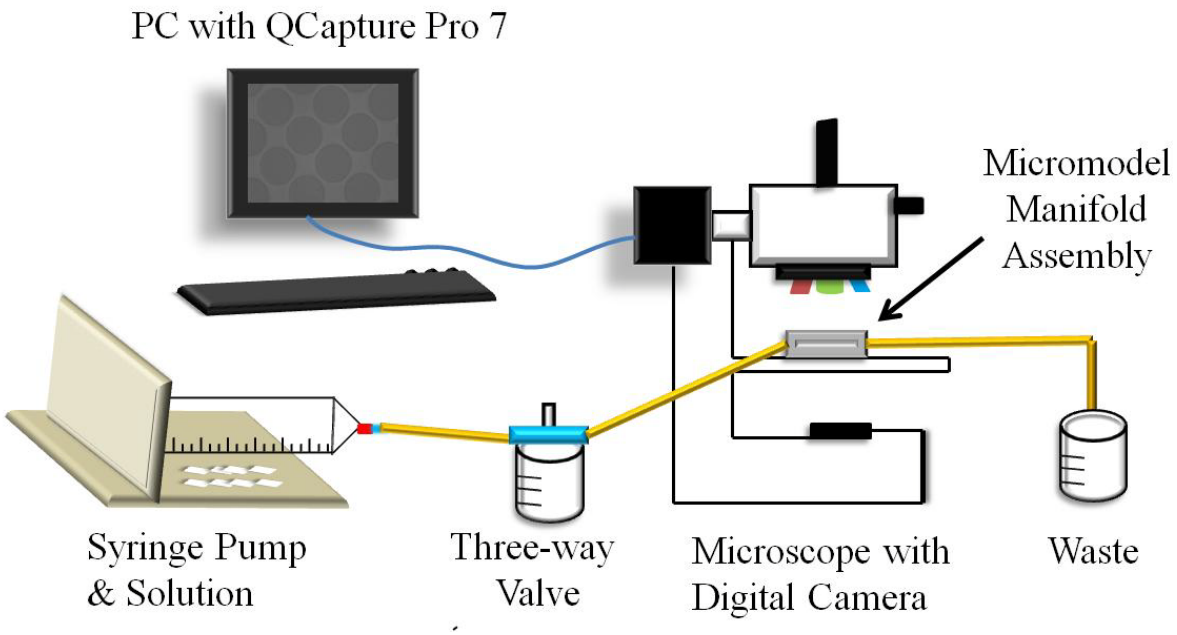

Figure 4.1. Schematic of micromodel system that includes the syringe pump, nanoparticle suspension, three-way valve, microscope and digital camera, computer with imaging software, micromodel and manifold assembly, and waste container.

4.2. Materials and Methods

4.2.1 Micromodel Fabrication

The micromodels were made from silicon wafers via standard photolithography procedures (described below in section 1.2) in a class-10 cleanroom at the University of Illinois, Urbana-Champaign (UIUC). A total of six micromodels are fabricated from one 100 mm (4 inch) wafer. The pore network of each micromodel was formed from a uniform distribution of cylindrical collectors measuring 100 µm in diameter and 20 µm in height. The pore-body and pore-throat diameters were 70 µm and 20 µm, respectively (Figure 4.2). The porosity of the micromodel was 0.455. Both inlet and outlet diameters were 0.8 mm.

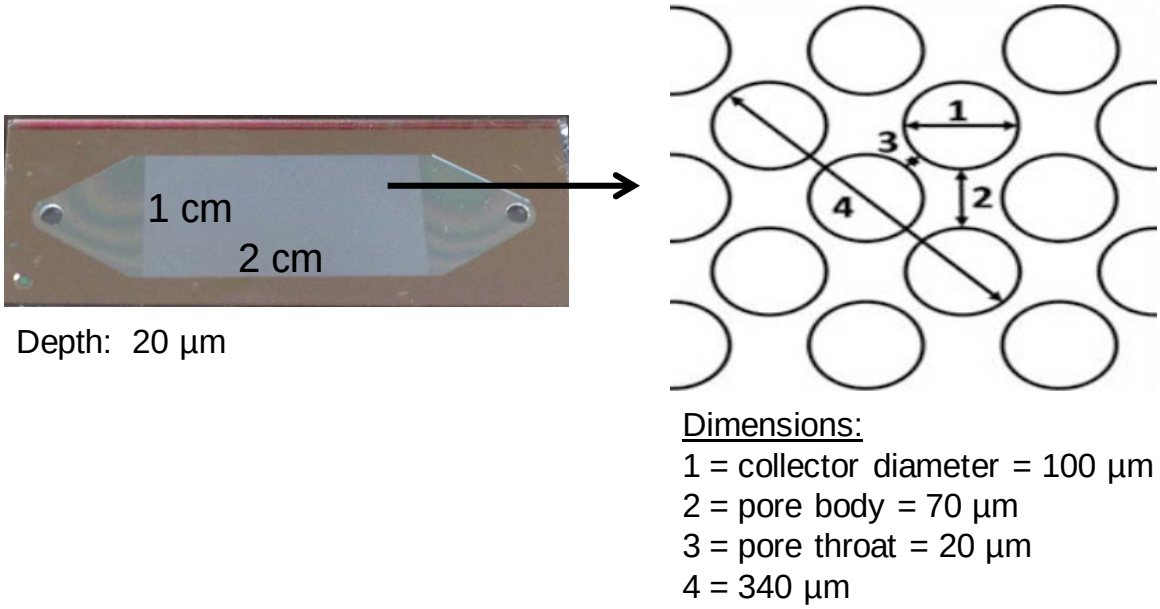

Figure 4.2. Dimensions of the micromodel and micromodel pore network.

4.2.2 Photolithography Procedures

The micromodel pore network was designed in AutoCAD and printed onto high-resolution transparencies. The patterns were transferred onto chrome masks and etched into each side of the same silicon wafer. The silicon wafer used in fabricating the micromodels was 100 nm in diameter and 0.5 mm thick and polished on both sides (Virginia Semiconductor, VA). Prior to fabrication, the silicon wafers were degreased and cleaned by deionized water, acetone, and isopropyl alcohol; then, the wafers were dried with nitrogen gas. The cleaned silicon wafer was coated with a thin layer (8 µm) of photoresist (PR) polymer, AZ 4620 (AZ Electronic Materials, NJ). The pore network pattern on the chrome mask was exposed onto the PR-coated wafer by ultraviolet light

(EV Group, AZ) for 12s at a wavelength of 405 nm. The PR exposed to the UV light was then removed with a PR developer solution, AZ 400K (AZ Electronic Materials, NJ). The exposed area was etched to a depth of 20 μm, which corresponds to the depth area through which the flow occurs by using an inductively coupled plasma-deep reactive ion etching (ICP-DRIE) system (Plasmatherm, FL). This process was done on the front side of the wafer for etching the features, and also on the back side to etch the inlet/outlet holes. Upon completion of etching, the wafer was cleaned using a PR stripper solution, AZ 400T (AZ Electronic Materials, NJ) at 150 ^{O}C, an acid solution (3:1 ratio of H_2SO_4:H_2O_2), and a base solution (5:1:1 ratio of DI water:H_2O_2:NH_4OH) at 150 ^{O}C. The cleaned wafer was then oxidized in a tube furnace chamber for 2hrs at 1100 ^{O}C. The wafer was again cleaned using the same base solution described above and dried with nitrogen gas. Finally, the porous media pattern features were sealed by anodically bonding it to a 100 mm diameter Pyrex glass wafer (Sensor Prep Services, IL) using a thermal-anodic bonder (EG Group, AZ). Using a dicing saw and blade (Disco Corporation, NH), the wafer was cut into the six individual micromodels.

4.2.3 Micromodel Experiment

The micromodel was housed in a custom-built aluminum manifold assembly (Vocademy, CA), which measures 4 square-inches for both the top and bottom plates; the top and bottom were ¼ in. and ½ in. thick, respectively (Figure 4.3).

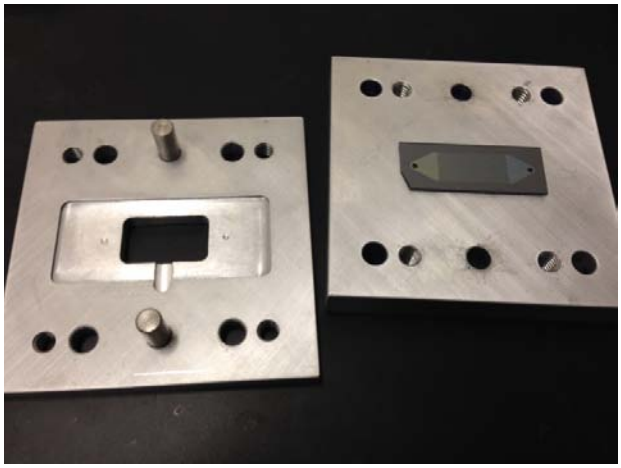

Figure 4.3. Manifold assembly (top and bottom plates) + micromodel.

The bottom plate of the manifold assembly houses inlet and outlet ports that direct fluid flow into and out of the micromodel while the top plate secures the whole system in place. This micromodel system was installed under a fluorescent microscope (Olympus BX-51, PA) using a 20x objective. Prior to each experiment, the micromodel was saturated with the KCl electrolyte via a slow-flow rate syringe pump (KDScientific, MA) through 0.18 mm diameter Teflon tubing (Upchurch, OK) that were connected to the inlet and outlet ports of the manifold assembly. LNP at a concentration of 10^{10} particles/mL in the desirable electrolyte were pumped into the micromodel at a flow rate of 1 µL/hr. This flow rate was selected based on a Peclet (Pe) number of 1, which is a comparable Pe value in column experiments. The Pe number measures the relative strength of fluid forces (advective to dispersive), and is defined by[19]

$$Pe = \frac{3A_f V_\infty a^3}{R^2 D_0} \qquad (1)$$

where A_f is the flow parameter, V is the uniform flow velocity, a is the particle radius, R is the radius of the collector surface, and D_0 is the diffusion coefficient. The concentration of particles was selected to ensure sufficient particles would be seen and quantified in images. For all experiments, pH of the suspensions was unadjusted (5.6±0.2). Experiments lasted for 30 minutes, with real-time images captured every minute through a charge-coupled device camera (QImaging Retiga Fast 1394, BC) and QCapture Pro 7 software (QImaging, BC). Images were saved and later analyzed to determine the attachment and deposition of LNP over time on the collector surfaces. The number of LNP that attached to six collector surfaces (based on the viewing area from the 20x objective) was counted from the saved images after 30 minutes of experimentation. The single collector removal efficiency (η) is the fraction of particles approaching collector that actually collide and was determined by[19]

$$\eta = \frac{I}{\pi R_C{}^2 u C_0} \tag{2}$$

where I is the average attachment rate of LNP on a cylindrical collector (I is determined by dividing the total number of attached LNP divided by the product of the number of collectors and time of experimentation), R_c is the radius of the collector, u is the approach velocity, and C0 is the concentration of LNP (particles/mL). Thus, the number of LNP can be quantified over the viewing area of collectors and expressed as the collector removal efficiency, η.

4.2.4 Nanoparticle Selection and Characterization

The model nanoparticle selected for a proof of concept demonstration of this micromodel set-up was a 20 nm carboxylate-modified fluorescent latex microsphere with a 505 nm excitation and 515 emission wavelengths (Life Technologies, NY, catalog number F-8787). According to the manufacturer, these latex nanoparticles (LNP) were manufactured using ultraclean polystyrene and high density carboxylic acids on their surface for increased particle stability. Additionally, these LNP were selected to allow for the direct comparison of nano-latex transport in the 2D micromodel vs. a 3D column[11]. LNP suspensions were prepared by diluting stock samples in KCl electrolyte (ACS Reagent Grade, Fisher Scientific) made with DI water of varying ionic strength (1, 3.16, 10, 31.6, and 100 mM) at unadjusted pH (5.6 ±0.2). The LNP concentration used was 10^{10} particles/mL. To disperse the suspensions, the LNP were sonicated (Transsonic 460/H, Barnstead Lab-Line, Melrose Park, IL) for ~2min and stirred prior to micromodel experimentation and particle characterization.

Electrokinetic characterization (zeta potential) and particle sizing (hydrodynamic diameter) measurements were conducted using a ZetaPals Analyzer (Brookhaven Instruments Corp, Holtsville, NY). Zeta potential was determined from the Smoluchowski equation, which is applicable when the Debeye length (thickness of the double layer) of a particle is much less than the particle size[20,19]. Particle sizing was measured using Dynamic Light Scattering (DLS) (Brookhaven Model-BI-9000AT, Holtsville, NY). The zeta potential and hydrodynamic diameters were determined from

the average of 5 runs, with each run lasting for two minutes. 2 mL of test samples were needed for all characterization experiments.

4.2.5 Micromodel Cleaning

Micromodel reuse was of significant interest since it is extremely expensive and fragile. Thus, a cleaning protocol was developed to clean the micromodel after each experiment. All steps should been done in the hood with double layer gloves and goggles. Upon completion of an experiment, the micromodel was removed from the manifold assembly. Then, it was placed into a beaker with 98% H_2SO_4 (~18M H_2SO_4) for 30min, using an evaporating dish to cover the beaker. Next, the H_2SO_4 was diluted from 18M to 9M into another beaker. Then, the micromodel was soaked into this solution for over 15 hours. Use DI water to clean the micromodel until the pH of micromodel is higher than 5. Also, a 3M H_2SO_4 solution was injected into the micromodel over 2 hours to wash the features and tubing. A specific flow rate pattern in the springe pump was applied: the first 30min is 1000 μL/hr, and the next 30min was switch to 10,000 μL/hr; this process was repeated several times. The purpose of this pattern is to eliminate all dead zones of collectors by increasing turbulence of the flow. After all the steps, the micromodel is cleaned and ready for reuse.

4.3 Results and Discussion

4.3.1 Micromodel Cleaning and Re-use

A critical piece of the micromodel application is the development of a cleaning protocol allowing for reuse. Extensive time was spent in fabricating the model, and since it is rather fragile, expensive, and originally designed to be disposable (i.e. one-time use per experiment), a cautious and rigorous cleaning procedure was needed. A systematic approach was carefully executed for various parameters tested during the cleaning stages. Such parameters tested included 1) flowrate for DI/electrolyte rinsing (100, 1,000, 2,500, 5000, 7,500, 10,000, and 20,000 μL/hr), 2) adjustment of pH for both DI water and electrolyte rinsing (unadjusted pH of 5.6; 7) via syringe pump, 3) duration of syringe pump rinsing (1, 5, 10, 15, 20, 25, 30, 45, and 60 min), 4) duration of syringe pump rinsing + sonication of micromodel/manifold assembly (1, 5, 10, 15, 20, 30, 45, and 60 min), and 5) length of time of acid wash (0.17, 0.5, 1, 2, 4, 12, 15, and 24 hrs). The goal of these rigorous cleaning procedures was to determine the shortest amount of time needed for rinsing and sonicating, and utilize the slowest flow rate possible. These conditions were of critical importance to ensure that there was no excess strain or pressure applied to the micromodel to cause it to break. Thus, as determined from these conditions, the safest and optimum cleaning parameters were: 10,000 μL/hr syringe pump flowrate, pH 7 of DI water/electrolyte, 30 min of sonication + DI/electrolyte rinsing, and 15 hours of acid bath washing. It is important to note that these cleaning protocols were optimized for LNP, and may need to be updated or revised for each subsequent type of nanoparticle used.

At the end of each micromodel experiment, the micromodel was removed and placed into a beaker with 18M H_2SO_4 for 30 min. Next, the micromodel was placed into another beaker with diluted (9M) H_2SO_4 for >15 hours. Upon acid rinsing, DI water was used to clean the micromodel (>20 rinses) until the pH of the it was greater than 5. To clean the tubing and further flush the micromodel, 3M H_2SO_4 was injected continuously for >2 hours at two variable flow rates of 1,000 µL/hr and 10,000 µL/hr, cycling every 30 minutes. This step was done to help eliminate dead zones of collectors due to more turbulent flow patterns. Upon acid rinsing, a final rinse with DI water was performed for >1 hr. To check if the micromodel was correctly cleaned, it was viewed under the microscope at all regions (inlet, middle area, outlet) and examined for any nanoparticles attached to the collector surfaces.

4.3.2 Chacterization of Latex Nanoparticles

The stability of the LNP was determined at a fixed concentration of 10^{10} particles/mL at unadjusted pH (5.6±0.2) across five different ionic strengths of KCl (1, 3.16, 10, 31.6, and 100 mM). Figure 3A below shows the hydrodynamic diameters and Figure 4B shows the zeta potentials measured. As seen from Figure 4A, the size of LNP increased as a function of ionic strength, ranging from ~150-400 nm. The increase in size with increasing ionic strength corresponds to the anticipated compression of the electrical double layer (EDL)[19-20]. Figure 4B shows the range of zeta potentials across the same conditions from the size data. Zeta potential values ranged from 30-45 mV, although this variation was statistically insignificant as they were within error of each other for 1, 3.16, and 10 mM KCl.

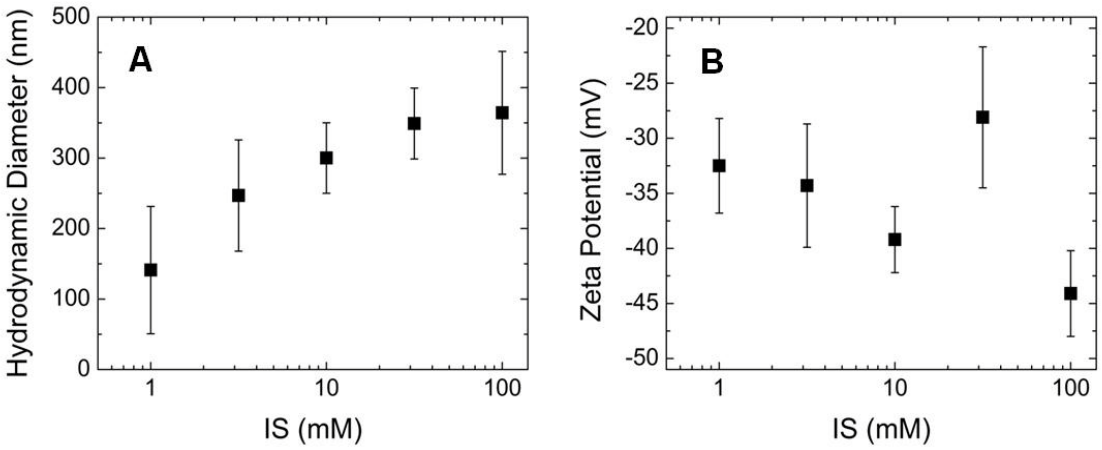

Figure 4.4. Hydrodynamic diameters (A) and zeta potentials (B) for LNP at a concentration of 10^{10} particles/mL in unadjusted pH (5.6±0.2) at five different ionic strengths of KCl (1, 3.16, 10, 31.6, and 100 mM).

The size and charge of the LNP were also measured as a function of pH ranging from 4-10 at 10^{10} particles/mL in 10 mM KCl. Figure 4.5A below shows the hydrodynamic diameters and Figure 4B shows the zeta potentials. As seen from Figure 5A, the size of the LNP was not independent (P = 0.03; ANOVA test run in Microsoft Excel, v. 2010) of pH and all remained in the range of 150±100 nm. However, a different trend was observed in Figure 4.5B with zeta potential. Zeta potential ranged anywhere between -20 mV (at pH 4) to -50 mV (pH 6, 9, and 10).

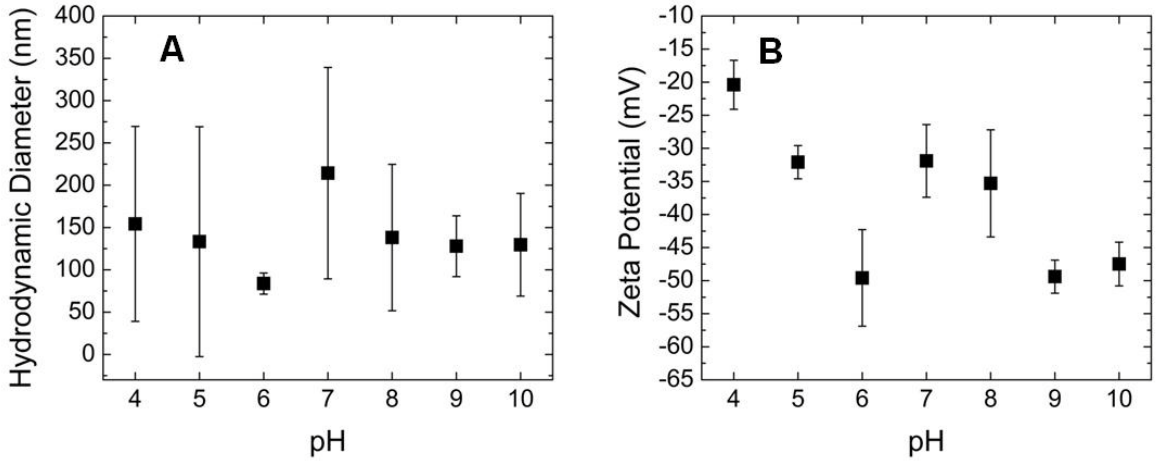

Figure 4.5. Hydrodynamic diameters (A) and zeta potentials (B) for LNP at a concentration of 10^{10} particles/mL in 10 mM KCl at various pHs (4, 5.6, 7, 8, 9, and 10).

4.3.3 Particle Counting and Single Collector Efficiency

The amount of deposited LNPs was counted over six collector surfaces (based on a viewing area of 350 x 450 µm, which allows for imaging six complete collectors) from time 0 - 30 min at a fixed concentration 10^{10} particles/mL and unadjusted pH over a range of ionic strengths (1, 3.16, 30, and 100 mM) of KCl. All images involving particle counting hereafter represent the most center, middle region of the 1 x 2 cm micromodel. These results are presented in Figures 4.6 through 4.9.

Figures 4.6 A, C, E, and G show an image of the six collectors at time 0 min before LNP injection with 1mM KCl. Figures 4.6 B, D, F, and H represent the same six collectors after 30 min of experimentation. As indicated by the arrows in Figure 4.6B, only two of the 6 collectors had any deposition, with only one particle over the entire

length of the experiment. Figures 4.6 C, E, and G follow the same format, showing the micromodel at time 0, prior to particle injection. Figure 6F shows multiple particles (total of 14) attaching over the six collectors after 30 min of particle injection in 31.6 mM KCl. Figures 4.6D and 4.5H in 10 and 100 mM KCl, respectively, show no LNP attaching to any of the collector surfaces. This phenomenon is agrees with the zeta potential data in Figure 6B previously. The zeta potential at 10 and 100 mM KCl were the most negative (greater than -40 mV), which indicates that the LNP were most stable in these conditions. In contrast, greatest deposition was observed at 31.6 mM KCl where the zeta potential was lowest (-25 mV). These trends indicate that attachment was greatest where zeta potential was less negative.

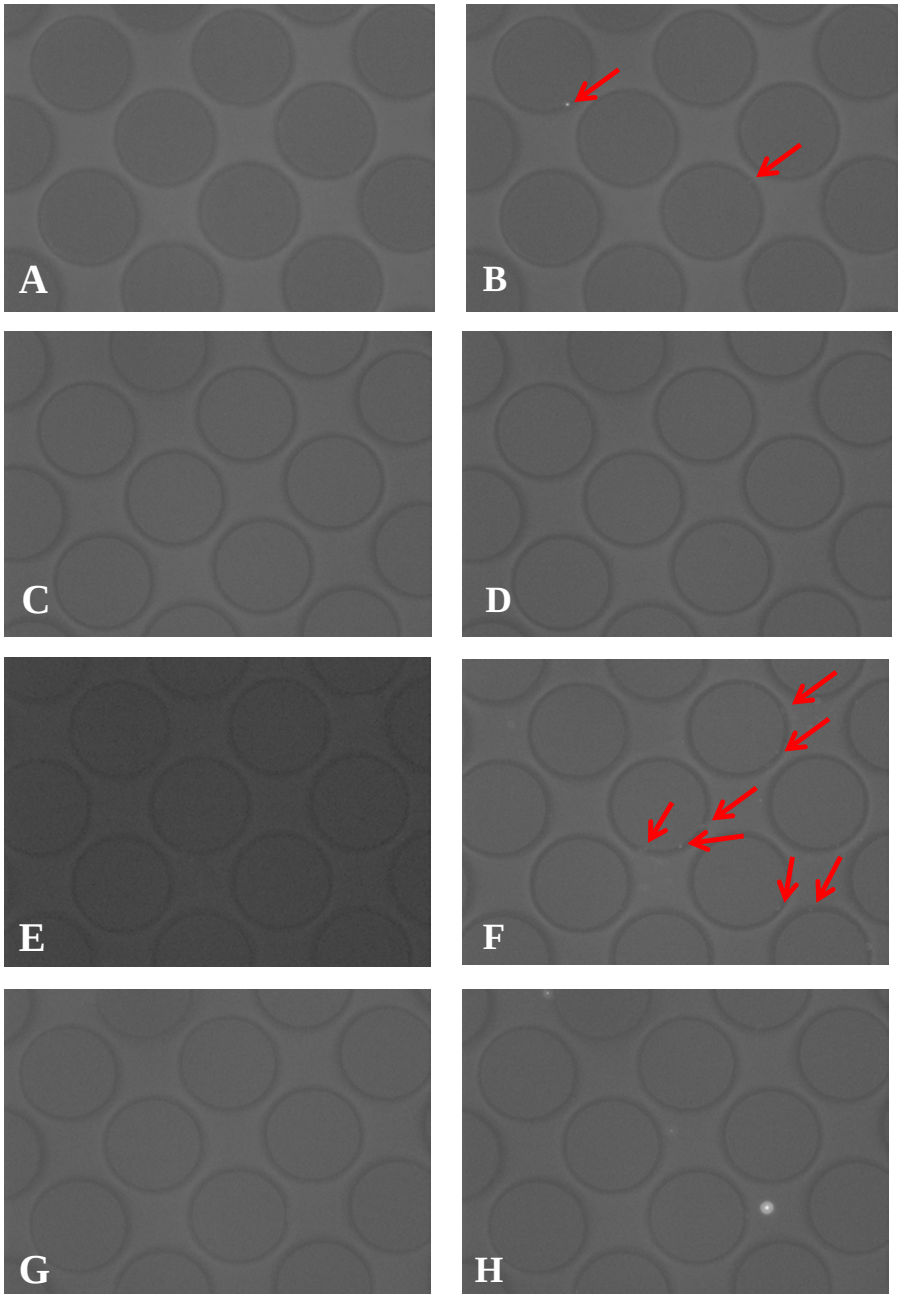

Figure 4.6. Micromodel experiment with QCapture Pro 7 imaging at time = 0 min (A, C, E, G) and 30 min (B, D, F, H) at 1 mM KCl (A & B), 10 mM KCl (C & D), 31.6 mM KCl (E & F), and , 100 mM KCl). All experiments had a fixed LNP concentration of 10^{10} particles/mL and were at unadjusted pH (5.6±0.2). The arrows in the images indicate locations of deposited particles onto collector grains.

Based on the number of LNPs deposited under the conditions of this study, a plot of single collector efficiencies (η) was constructed (Figure 4.7). As seen from Figure 4.7, there was no clear trend between η and IS. However, η was observed at ionic strengths of 1 mM KCl (~1 x 10^{-19}) and more notably at 31.6 mM KCl (~2.3 x 10^{-19}). At 10 and 100 mM, no LNP attached to any collector surface, thus resulting in a single collector efficiency of zero. These trends, though, agree with the zeta potential data (Figure 4.4B) and the images (Figures 4.6 B, D, F, and H): the less negative zeta potentials (1 and 31.6 mM KCl) had some attachment, whereas the conditions at which the LNPs had the most negative zeta potentials (10 and 100 mM KCl) there was no attachment. In essence, due to the overall low total amount of LNP attached in the entire porous network, attachment was considered negligible for all scenarios. A more favorable condition (i.e. with lower pH, higher flow rate, and/or divalent electrolyte solution) would result in more LNP attachment onto the collector surfaces.

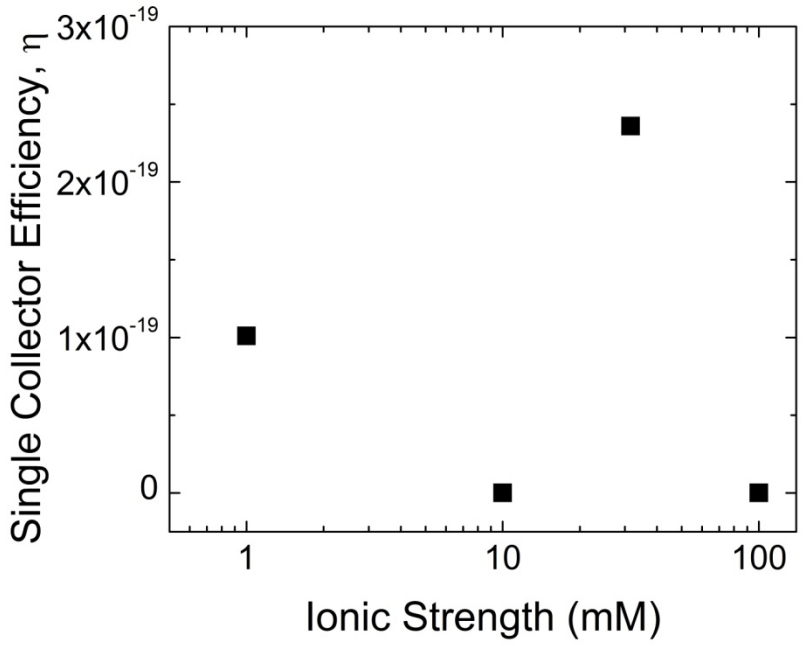

Figure 4.7. Single collector efficiency, η, as a function of ionic strength. Conditions were as follows: 10^{10} particles/mL, unadjusted pH (5.6±0.2), and four ionic strengths of KCl (1, 10, 31.6, and 100 mM). Each micromodel experiment at these conditions was conducted once.

4.3.4 Comparison of Micromodel (2D) to Column (3D)

Previous work from Quevedo et al. (2012)[11] employed the use of LNPs in a column experiment. This previous study provided the basis for comparison between our 2D micromodel and their reported results working with a 3D macro-scale column. To be able to account for the variable geometries between the two systems and relate them to one another, a Peclet value of 1 was determined for their column. Consequently, the micromodel experiments were also conducted at a Peclet value of 1, allowing for direct comparison between the two systems. Figure 4.8 below is a sample of their attachment

data from the column experiments at pH 7 and 1 mM KCl. The attachment efficiency of all nanoparticles increased from 10^{-3} to 10^{-1} as a function of increasing ionic strength. According to their zeta potential data, attachment increased with decreasing zeta potential; rather, particles attached to the collector surfaces when the particles were less stable. For the micromodel experiments, similar trends were seen where particle attachment was most prevalent with less negative zeta potential (31.6 mM KCl, followed by 1 mM KCl). However, a greater magnitude of removal was seen in all conditions in the column studies, indicating that removal occurred more in the 3D pore spaces through straining, blocking, or wedging[19]. Since a favorable condition (i.e. maximum attachment of particles) was not achieved in our micromodel study to date, attachment efficiency, α, was not determined since it is ratio of η/η_{fav}. However, typical values of α in a micromodel have been reported to range anywhere from 10^{-3} to 10^{-1} when using non nano-sized particles[16,17]. For a true comparison between the micromodel and column experiments, α must be determined to relate both systems. For our study, initial comparisons were made by comparing relative sensitivity to the varying ionic strengths of KCl.

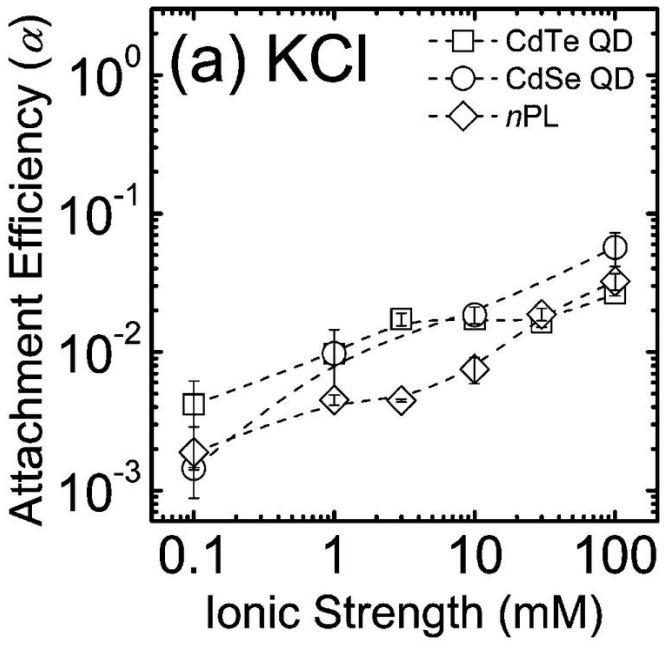

Figure 4.8. Attachment efficiencies calculated as a function of ionic strength for three different nanoparticles in KCl at pH 7. Experiments were conducted using columns packed with clean quartz-sand. This figure was taken directly from the original authors Quevedo et al. (2012)[11] for comparison purposes with our study.

4.4 Conclusions

This research has demonstrated that fabricated silica micromodels 1) provide considerable insight into the quantification of nanoparticles onto collector surfaces, and 2) these 2D flow cells can be used in tandem with 3D macro-scale column experiments for rich, mechanistic studies. Additionally, physico-chemical reactions, mechanisms, and intermolecular forces may be examined in a close-up 2D pore-scale system. This new approach involving the micromodel and enumeration techniques associated with it has great promise and capacity as an, innovative tool for quantitatively studying nanoparticle removal mechanisms in the absence of complex pore structures in real-time.

4.5 Acknowledgements

This research was supported by the National Science Foundation under Grant No. CBET-0954130. Any conclusions, findings, recommendations, or suggestions expressed in this study are those of the authors and may not reflect the views of the National Science Foundation. We would like to acknowledge Dr. Yuanyuan Liu, Nanxi Lu, and Professor Thanh Nguyen at the University of Illinois, Urbana-Champaign (UIUC) for their demonstration and insight regarding micromodel development and application. Additionally, we would like to thank the Miki Takagi, Michael Hansen, Dr. Glennys Mensing and the rest of their cleanroom staff at UIUC for the teaching and access to the cleanroom 7 days/week. We would like to acknowledge Dr. Brian Thibeault and Ning Cao at the University of California, Santa Barbara Nanotech cleanroom facility for their services in dicing the micromodels. Lastly, we would like to thank and acknowledge Chen Chen, graduate student researcher, and undergraduate researchers Stacey Nwagbara, Christine Brown, and Corey Luth for their helpful contributions to micromodel experimentation and characterization data collection.

4.6. References

1. Dunphy Guzmán, K. A.; Taylor, M. R.; Banfield, J. F., Environmental Risks of Nanotechnology: National Nanotechnology Initiative Funding, 2000−2004. *Environmental Science & Technology* **2006,** *40* (5), 1401-1407.

2. Wiesner, M. R.; Lowry, G. V.; Alvarez, P.; Dionysiou, D.; Biswas, P., Assessing the Risks of Manufactured Nanomaterials. *Environ. Sci. Technol.* **2006,** *40* (14), 4336-4345.

3. Mueller, N. C.; Nowack, B., Exposure Modeling of Engineered Nanoparticles in the Environment. *Environmental Science & Technology* **2008,** *42* (12), 4447-4453.

4. Kiser, M. A.; Westerhoff, P.; Benn, T.; Wang, Y.; Pérez-Rivera, J.; Hristovski, K., Titanium Nanomaterial Removal and Release from Wastewater Treatment Plants. *Environmental Science & Technology* **2009,** *43* (17), 6757-6763.

5. Chowdhury, I.; Hong, Y.; Honda, R. J.; Walker, S. L., Mechanisms of TiO2 nanoparticle transport in porous media: Role of solution chemistry, nanoparticle concentration, and flowrate. *J. Colloid Interface Sci.* **2011,** *360* (2), 548-555.

6. Keller, A. A.; Wang, H.; Zhou, D.; Lenihan, H. S.; Cherr, G.; Cardinale, B. J.; Miller, R.; Ji, Z., Stability and Aggregation of Metal Oxide Nanoparticles in Natural Aqueous Matrices. *Environ. Sci. Technol.* **2010,** *44* (6), 1962-1967.

7. Lanphere, J. D.; Luth, C. J.; Walker, S. L., Effects of Solution Chemistry on the Transport of Graphene Oxide in Saturated Porous Media. *Environmental Science & Technology* **2013,** *47* (9), 4255-4261.

8. Hong, Y.; Honda, R. J.; Myung, N. V.; Walker, S. L., Transport of Iron-Based Nanoparticles: Role of Magnetic Properties. *Environ. Sci. Technol.* **2009,** *43* (23), 8834-8839.

9. Jaisi, D. P.; Elimelech, M., Single-Walled Carbon Nanotubes Exhibit Limited Transport in Soil Columns. *Environmental Science & Technology* **2009,** *43* (24), 9161-9166.

10. Lecoanet, H. F.; Wiesner, M. R., Velocity Effects on Fullerene and Oxide Nanoparticle Deposition in Porous Media. *Environ. Sci. Technol.* **2004,** *38* (16), 4377-4382.

11. Quevedo, I. R.; Tufenkji, N., Mobility of Functionalized Quantum Dots and a Model Polystyrene Nanoparticle in Saturated Quartz Sand and Loamy Sand. *Environmental Science & Technology* **2012,** *46* (8), 4449-4457.

12. Baumann, T.; Werth, C. J., Visualization and Modeling of Polystyrol Colloid Transport in a Silicon Micromodel. *Vadose Zone J.* **2004,** *3* (2), 434-443.

13. Auset, M.; Keller, A. A., Pore-scale visualization of colloid straining and filtration in saturated porous media using micromodels. *Water Resources Research* **2006,** *42* (12), W12S02.

14. Keller, A. A.; Auset, M., A review of visualization techniques of biocolloid transport processes at the pore scale under saturated and unsaturated conditions. *Advances in Water Resources* **2007,** *30* (6–7), 1392-1407.

15. Willingham, T. W.; Werth, C. J.; Valocchi, A. J., Evaluation of the Effects of Porous Media Structure on Mixing-Controlled Reactions Using Pore-Scale Modeling and

Micromodel Experiments. *Environmental Science & Technology* **2008,** *42* (9), 3185-3193.

16. Liu, Y.; Zhang, C.; Hilpert, M.; Kuhlenschmidt, M. S.; Kuhlenschmidt, T. B.; Nguyen, T. H., Transport of Cryptosporidium parvum Oocysts in a Silicon Micromodel. *Environmental Science & Technology* **2012,** *46* (3), 1471-1479.

17. Liu, Y.; Zhang, C.; Hu, D.; Kuhlenschmidt, M. S.; Kuhlenschmidt, T. B.; Mylon, S. E.; Kong, R.; Bhargava, R.; Nguyen, T. H., Role of Collector Alternating Charged Patches on Transport of Cryptosporidium parvum Oocysts in a Patchwise Charged Heterogeneous Micromodel. *Environmental Science & Technology* **2013,** *47* (6), 2670-2678.

18. Lu, N.; Bevard, T.; Massoudieh, A.; Zhang, C.; Dohnalkova, A. C.; Zilles, J. L.; Nguyen, T. H., Flagella-Mediated Differences in Deposition Dynamics for Azotobacter vinelandii in Porous Media. *Environmental Science & Technology* **2013,** *47* (10), 5162-5170.

19. Elimelech, M.; Jia, X.; Gregory, J.; Williams, R., *Particle Deposition & Aggregation: Measurement, Modelling and Simulation*. Elsevier Science: 1998.

20. Gregory, J., *Particles in Water: Properties and Processes*. Taylor & Francis: 2005.

Chapter 5

Summary and Conclusions

The overall scope of this doctoral research was to investigate the fundamental mechanisms and phenomena governing the removal of engineered nanomaterials in engineered systems. Specifically, this study identified the capacity of traditional drinking water treatment processes to remove a model nanoparticle, TiO_2, and to fabricate a 2D micromodel to allow for comparative studies in a column. An effort was made to simulate a range of actual conditions that would be faced in a water treatment scenario. We varied the water sources tested, range of chemistries and constituents that would be present, and the type and dose of coagulants used. Even though the nanoparticle concentration used in the jar test experiments was unrealistic, it allowed for consistent quantitative measurements and repeatability between experiments, especially when using the spectrophotometer and ZetaPals analyzer. With the experiments optimized at higher nanoparticle concentrations and a successful scaled-down approach, future work for using lower (i.e. environmentally relevant concentrations <1 mg/L) will be merited.

In Chapter 2, there was evidence that typical primary treatment (coagulation, flocculation and sedimentation) can effectively remove TiO_2 nanoparticles within the range of concentrations tested. Additionally, it was demonstrated that the total removal capacity at the scaled-down level resulted in the same removal capacity as the conventional scale system with ≥1-log removal for all three coagulants. Also, the ideal choice of coagulant is dependent on the water source type. From the results, $FeCl_3$ proved to be more effective in total particle removal in AGW (> 95%) than in ASW (< 70%). Overall, $FeSO_4$ performed more effectively in ASW at all four TiO_2

concentrations tested (> 91%) than in AGW (>90 % at 50 and 100 mg/L; but 60-80% at 10 and 25 mg/L, respectively). Moreover, $Al_2(SO_4)_3$ was effective in both waters with similar removal results (nearly 100%). Based on the concentrations of metal coagulant used in this study, it is anticipated that removal via sweep flocculation is the dominant mechanism in particle removal. Furthermore, the effect of nanoparticle concentration was significant. In general, the higher TiO_2 concentrations (50 and 100 mg/L), the more effective the removal was when compared to the lower concentrations (10 and 25 mg/L). Several mechanistic phenomena, including electrostatic repulsion, bridging, charge reversal, complexation, helped describe removal effectiveness. Additionally, the source water impacts both the pH and ionic strength, and subsequently, affects the stability of the particles. The more acidic the solution is, the greater the zeta potential, and thus, a lower removal efficiency is observed. The decrease in pH observed in both source waters is due to chemical reactions associated with the metal coagulants.

In Chapter 3, it was determined that factors such as ionic strength, solution chemistry, and water type, significantly impacted the removal and stability of TiO_2. In addition, the impact of key environmental factors such as the presence of humic acids and particle coating hindered total particle removal. Bare TiO_2 was removed the most effectively, while DMSA-particle coating and SRHA enhanced particle stability, making removal less effective. Based on colloidal literature, it is known that increasing the salt concentration in solution screens the repulsive electrostatic interactions between particles through compression of the electrical double layer that surrounds a charged particle. This

research observed how both nanoparticle coating and NOM influenced stability of the particles. The more stable the particles were (smaller magnitude of zeta potential), the greater the aggregate size became. This suggests a substantial amount of nanomaterials will stay suspended as the water stream continues onto the filtration stage. Our study has systematically considered these many but significant and complex factors when investigating TiO_2 removal. Understanding these mechanisms will not only lead to enhanced effectiveness and optimization of experimental parameters during the particle removal process in groundwater or subsurface environments, but also help inform practitioners of best practices to treat them in facilities.

Chapter 4 described a novel and innovative approach to help understand the fundamental mechanisms that govern attachment of latex polystyrene nanoparticles in a 2D micromodel flow cell. Findings from this study showed that latex nanoparticle quantification and deposition were a function of pH, ionic strength, and flowrate. Attachment of particles onto collector surfaces was observed in two conditions at 1 and 31.6 mM KCl. The corresponding zeta potentials and size for those two conditions were less stable (i.e. less negatively charged) than other scenarios. Essentially though, attachment was zero in this study since no favorable condition was achieved, and the total of attached particles in 1 and 31.6 mM KCl was very low. All experiments were done at unadjusted pH or 7 where particles remained stable throughout. However, this research has demonstrated that fabricated silica micromodels provide considerable insight into the quantification of nanoparticles onto collector surfaces, and how these 2D micromodel

flow cells can be used in conjucntion with 3D macro-scale column experiments for mechanistic studies. Additionally, physico-chemical reactions, mechanisms, and intermolecular forces may be examined in a close-up visualization 2D pore-scale system. This new approach involving the micromodel and its associated enumeration techniques has great promise and capacity as an innovative tool for quantitatively studying nanoparticle removal mechanisms in the absence of complex pore structures in real-time capability. Ultimately, this work has provided a combination of tools that allows for the investigation of nanoparticle removal in water treatment. A substantial range of parameters and scenarios have been tested - albeit future studies are merited - that suggests particle removal is feasible under optimized treatment conditions.